Channeling Through Two Stacked Guanine Quartets of One and Two Alkali Cations in the Li + , Na + , K + and Rb + Series. Assessment of the Accuracy of the SIBFA Anisotropic Polarizable Molecular Mechanics Potential

Nohad Gresh, Sehr Naseem-Khan, Louis Lagardère, Jean-Philip Piquemal, Judit E. Sponer, Jiri Sponer

Channeling Through Two Stacked Guanine Quartets of One and Two Alkali Cations in the Li^+, Na^+, K^+ and Rb^+ Series. Assessment of the Accuracy of the SIBFA Anisotropic Polarizable Molecular Mechanics Potential.

[1]Nohad Gresh*, Sehr Naseem-Khan, Louis Lagardère, Jean-Philip Piquemal
[2]Judit E. Sponer,[2,3] Jiri Sponer*[2,3]

[1]Laboratoire de Chimie Théorique, Sorbonne Universités, UPMC, UMR7616 CNRS, Paris, France
[2]Institute of Biophysics, Academy of Sciences of the Czech Republic, Kralovpolska 135, 612 65 Brno, Czech Republic
[3] CEITEC – Central European Institute of Technology, Masaryk University, Campus Bohunice, Kamenice 5, 625 00 Brno, Czech Republic

e-mail addresses: gresh@lct.jussieu.fr (NG); sponer@ncbr.muni.cz (JS).

Abstract.

Stacking of guanine quartets (GQ) can trigger the formation of DNA or RNA quadruple helices, which play numerous biochemical roles. The GQs are stabilized by alkali cations, mainly K^+ and Na^+, which can reside in, or channel through, the central axis of the GQ stems. Further, ion conduction through GQ wires can be leveraged for nanochemistry applications. G-quadruplex systems have been extensively studied by classical molecular dynamics (MD) simulations using pair-additive force fields or by quantum-chemical (QC) calculations. However, the non-polarizable force fields are very approximate while QC calculations lack the necessary sampling. Thus, ultimate description of QG systems would require long-enough simulations using advanced polarizable molecular mechanics (MM). However, to perform such calculations, it is first mandatory to evaluate the method's accuracy using benchmark QC. We report such an evaluation for the SIBFA polarizable MM, bearing on the channeling (movement) of an alkali cation (Li^+, Na^+, K^+, or Rb^+) along the axis of two stacked G quartets interacting with either one or two ions. The QC energy profiles display markedly different features depending upon the cation but can be retrieved in the majority of cases by the SIBFA profiles. An appropriate balance of first-order (electrostatic and short-range repulsion) and

second-order (polarization, charge-transfer and dispersion) contributions within ΔE is mandatory. With two cations in the channel, the relative weights of the second-order contributions increase steadily upon increasing the ion size. In the G8 complexes with two K^+ or two Rb^+ cations, the sum of polarization and charge-transfer exceeds the first-order along terms for all ion positions.

Introduction.

The present study bears on the channeling of one and two alkali cations between two stacked guanine quartets (GQ). It is motivated by the growing evidence for the involvement of G quartets in a wealth of biological events [for a recent review, 1]. Thus GQs promote the formation of quadruple helices in telomeric DNA[2] and in G-rich sequences in the genome[3,4] Evidence is mounting for the involvement in GQs in human genome regions that are essential for replication, such as *c-myc*[5], *bcl-2* [6], *c-kit* [7], VEGF [8], and Refs. therein] but also in viruses [9, 10]. GQs thus constitute an emerging target for the design of novel chemotherapeutic molecules which can stabilize the quadruple helix and inhibit telomerase or interfere with transcription [11-15]. GQs are endowed with electron transport [16, 17], photoelectronic properties of potential interest in nanochemistry [18, 19] while GQ-based nanowires are endowed with ion-conducting properties [20, 21].

GQ quadruple helices have been investigated by X-ray crystallography [22, 25] and Refs. therein, high-resolution NMR [23, 24, 26], and molecular dynamics [27-30]; for a review, see Ref. 31. G-quartets have been studied in several high-level ab initio quantum chemistry (QC) calculations bearing on their electronic and cation-binding properties [32, 33], the ranking of competing conformers [34] and the cooperativity of their self-associations [35, 36]. Extensions of QC analyses to novel halogenated derivatives of deazaguanine and their complexes with Na^+ and K^+ were recently reported [32].

The alkali cations Na^+ and K^+ can act as important contributors to the stability of stacked G quartets, owing to their propensity to bind in-between two successive GQs. GQ-containing quadruple helices can interconvert between several alternative forms with short-lived intermediates, the detection of which can evade direct experimental measurements. Long-duration molecular dynamics could be ideally suited for such explorations and have already provided insight to unravel candidate interconversion pathways [30]. There are, however

acknowledged limitations to 'classical' molecular mechanics (MM) force-fields for such applications, which could be magnified in the presence of metal cations. Thus a recent study investigated the channeling of a monovalent cation along the Z axis of two and three stacked G quartets, in the presence of another cation fixed along this axis at 1.1 Å above the topmost quartet [37]. The MM energy profile differed significantly from the DFT-D3 one upon moving the cation closer to the fixed one. This was ascribed to the lack of an explicit polarization contribution (E_{pol}): a raise of the inter-cation electrostatic repulsion ought to be, to a significant extent, compensated for by a concomitant increase of E_{pol}, since the polarizing field exerted by both cations on the G quartets increases as the two cationic charges get closer together, yet this contribution is absent from classical MM. This then raises an essential issue: how well, by contrast, would anisotropic polarizable molecular mechanics (APMM) profiles fare with respect to the QC profiles? Owing to the highly polar and polarizable nature of guanine, cation-bound G quartets constitute a very revealing benchmark for the accuracy of APMM procedures. Their stabilization involves the interplay of multiply H-bonded, stacked, and cation-ligand interaction and the onset of non-additivity of the total intermolecular interaction energies (ΔE). Evaluation of the APMM accuracy in light of these tests is also part of the construction of polarizable potentials for DNA and RNA [38] owing to the prevalence and constant interplay of such effects. The present GQ tests will bear on the SIBFA APMM procedure [39] and is a continuation of two preceding works. The first bore on the calibration of the alkali cation series (Li^+, Na^+, K^+, Rb^+, Cs^+) and QC validation tests of a series of their polyligated complexes [40]. The second bore on several stacked and H-bonded complexes of cytosine and guanine [41]. The first polarizable molecular mechanics study bearing on the selective entrapment of alkali cations between two G quartets was a SIBFA study published in 1986 [42]. Each quartet was then however considered as one entity, while in the present study the individual entities are the bases and the cations.

A CPK representation of the two stacked G quartets and of the channeling cation in its successive positions are represented in Figure 1. The unmoving cation is on the top of the Z axis. Throughout this study we retain for both QC and SIBFA computations the idealized stacked GQ geometry constructed in Ref. [37]. Owing to the validation purpose of the present study, relaxing the geometries by energy-minimization or molecular dynamics would be unrealistic and untimely, as it would ignore the averaging effect of additional stacked G quartets, of other channeling cations and the effects of the environments: this will be very

continuation of the present work. Note that the geometries taken from ref. [37] are very well prepared and should be sufficient for the purpose of the benchmark computations.

The organization of this paper is as follows. We first consider one G quartet and compare SIBFA and QC results at both HF and DFT-D3 levels. GQ is emblematic of cyclic, multiply H-bonded complexes with strong anticipated cooperativity. Energy Decomposition Analyses (EDA) performed at the HF level will enable to compare the summed values of each individual energy contribution in the six guanine dimers to its value in the quartet. We thus trace back the share of each contribution of ΔE(QC) in the total cooperativity, and how well it is reflected in the context of the SIBFA. Another test bears on the stacking of two half-quartets. We retain in the first quartet one H-bonded guanine dimer, denoted as G1-G2, and in the second quartet one of the two H-bonded dimers with maximal overlap with G1-G2, denoted as G1'-G2'. This will enable to evaluate non-additivity in mixed H-bonded/stacked complexes: could cooperativity now possibly revert into anticooperativity? Such analyses are limited to four guanines as larger-sized complexes are not amenable to EDA with large basis sets.

We next consider the complex of two stacked G quartets. It involves two extensive surfaces, each guanine of the first quartet being involved in non-remote stacking interactions with two guanines of the second quartet, whence a total of eight such interactions. Two stacked G quartets total twenty-eight simultaneous H-bonded or stacking guanine-guanine interactions, whether close or remote. Could an acceptable match of ΔE(SIBFA) to ΔE(QC) still be obtained?

Following these preliminary validations, we consider the channeling of one alkali cation, Li^+, Na^+, K^+, and Rb^+ along the Z axis. We follow the same trajectory as in the original paper [37]. It starts from a Z= -1.1 Å position below the first quartet and ends at Z= 2.5 Å above it, namely 0.8 Å below the second quartet. The same trajectory is recomputed, now in the presence of a second cation, the position of which is fixed at 1.1 Å above the second quartet. The shortest M^+-M^+ distance of approach is thus 1.9 Å. The first series of SIBFA vs. QC comparisons are reported at the HF level and with HF-derived multipoles and polarizabilities for SIBFA calculations. The second series of comparisons is at the DFT-D3 level and, for the SIBFA calculations, with DFT-derived multipoles and polarizabilities and the inclusion of an explicit dispersion contribution. We conclude with perspectives of MD applications to GQ-based channels and their alkali cation complexes.

Procedure.

Quantum-Chemistry (QC) calculations. The QC calculations used the cc-pVTZ(-f) basis set [43, 44] since the studied complexes on account of their sizes were not amenable to aug-cc-pVTZ(-f) calculations. A triple-dzeta basis set was used on K^+ [45]. The Stuttgart effective core potential [46] was used on Rb^+. Energy Decomposition Analyses (EDA) resorted to the RVS analysis due to Stevens and Fink [47] and coded in the GAMESS-US package [48]. Calculations at the correlated level used the B97-D3 energy functional augmented with the dispersion correction by Grimme et al. [49.] Some DFT calculations were also performed with the B3LYP functional [50, 51]. The DFT calculations were done with the G09 package [52].

SIBFA calculations. In the SIBFA procedure [39,] the intermolecular interaction energy is computed as the sum of five contributions: electrostatic multipolar (E_{MTP*}), short-range repulsion (E_{rep}), polarization (E_{pol}), charge transfer (E_{ct}), and dispersion (E_{disp})

$$\Delta E_{TOT} = E_{MTP*} + E_{rep} + E_{pol} + E_{ct} + E_{disp}$$

E_{MTP*} is computed with distributed multipoles (up to quadrupoles) derived from the QC molecular orbitals precomputed for each individual molecule using the Generalized Multipole Analysis (GDMA) method by Stone [53]. It is augmented with a penetration term [54, 55]. The anisotropic polarizabilities intervening in the expression of E_{pol} are distributed on the centroids of the localized orbitals (heteroatom lone pairs and bond barycenters) using a procedure due to Garmer and Stevens [56]. E_{rep} and E_{ct}, the two short-range repulsions, are computed using representations of the molecular orbitals localized on the chemical bonds and on localized lone-pairs [55, 57]. E_{disp} is computed as an expansion into 1/R**6, 1/R**8, and 1/R**10, and also embodies an explicit exchange-dispersion term [58].

We have also calibrated the short-range cation-cation repulsion, as it was found that at shorter M^+-M^+ distances, the sole electrostatic repulsion was insufficient. The calibration bore on the atom-pair multiplicative factor of E_{rep}, denoted PK_{IJ}, where I and J denote the atomic numbers of the two atoms concerned. It was done on the basis of EDA computations on the M+-M+ diatomic complexes, to match the radial dependency of E_{rep} in a range of distances between 2.0 and 3.0 Å. The multiplicative factors are PK_{Li-Li} =1.0, PK_{Na-Na} =9.0, PK_{K-K} =300.0, and PK_{Rb-Rb} =685. Apart from this point, we use the same cation parameters as those derived in 2015 [40].

The multipoles and polarizabilities at the HF and DFT levels are those derived in the context of our above-mentioned study on the cytosine and guanine complexes [41]. The general parameters were those previously derived on the basis of EDA on model complexes with the aug-cc-pVTZ(-f) basis by Devereux et al. [59] with the automated I-NoLLS (Interactive, nonlinear least squares) procedure [60]. Following [El Khoury et al., submitted] we use an improved representation of the sp^2 lone pairs on O6 and of the sp lone pairs on N7 and N3, 'smearing' them partially on both sides of the guanine plane. The in-plane component of the N7 and N3 lone pairs retains an electron population of 1.45, while each out-of-plane component, extending the external bisector of the nitrogen perpendicular to the plane, has an electron population of 0.275. The in-plane component of each O6 sp^2 lone-pair retains an electron population of 1.70, and there are two smeared components each with an electron population of 0.30, above and below the C=O bond. Such populations, together with the internal coordinates of the smeared lone-pairs, were fit to improve the radial dependencies of E_{rep}(SIBFA) compared to E_{exch}(RVS) upon in- and out-of-plane variations of the approach of a Zn(II) probe to O6 and N7 [Naseem-Khan et al., to be published]. We denote as E_1 the sum of the two first-order contributions E_C and E_{exch} (QC) and E_{MTP} and E_{rep}(SIBFA), and by E_2 the sum of the two second-order contributions E_{pol} and E_{ct}.

Non-Covalent Interaction (NCI) analyses. The NCI procedure [61, 62] is based on the study of the reduced density gradient as a function of density. It enables to visualize interaction zones between two molecules and gives access qualitatively to the magnitude of these interactions.

Results.

1. Stabilization energies in the G quartet, the stacked half-quartet, and in two stacked G quartets.

a) G quartet. Tables 1 report the results of the QC and SIBFA intermolecular interaction energies at the HF and correlated levels respectively.

HF results. The RVS procedure enables to trace back the origin of cooperativity by comparing the value of each ΔE contribution to the sum of its values in the six guanine dimers considered separately. The same comparisons are reported for SIBFA. ΔE(HF) is overestimated by ΔE(SIBFA) by 4.5 kcal/mol out of 50. This is due to both E_{MTP} and E_{rep} within E_1, each accountable for 2.1 kcal/mol out of app. 65 and 40 respectively. These overestimations occur in the four H-bonded dimers, amounting to 0.6 kcal/mol out of 16 and 10 for E_{MTP*} and E_{rep}, respectively. These errors could appear of lesser importance, but each is multiplied by four upon passing to the quartet. Shortcomings of E_{MTP*} could be due to instabilities in the GDMA procedure to derive distributed multipoles in the case of highly conjugated anionic ligands with diffuse functions, rendering them very sensitive to the choice of input parameters to derive them from the molecular orbital, namely the effective H radii and the switch function [53]. Towards deriving less sensitive multipoles, newly-emerging alternatives to GDMA are being considered, such as the Iterative Stockholder Analysis (ISA) [63, 64] and Gaussian Electrostatic Multipoles (GEM) [65, 66]. Their use will be reported elsewhere. E_{rep} is in turn impacted by the multipolar distribution as it has a prefactor which depends upon the monopolar charges of the interacting atoms. At present we move forward and leave aside these shortcomings. As shown below, upon passing to correlated levels, correlated multipoles afford a much closer match of SIBFA to QC than at the HF level. Furthermore, E_2(SIBFA) gives a closer match to its RVS counterpart than E_1, and it is E_2 that is responsible for the non-additivity of ΔE, δE_{nadd}, a critical element in the stacked G quartet-cation complexes. What is the amplitude of δE_{nadd}(QC), and could it be satisfactorily accounted for? Table 1 also reports the values of ΔE and its contributions in each of the six guanine-guanine dimer complexes, denoted G1-G2 to G3-G4. There are four equivalent doubly H-bonded dimers, G1-G2, G1-G4, G2-G3, G3-G4, and two non H-bonded dimers, G1-G3 and G2-G4. The summed values correspond to four times the values of one H-bonded dimer plus twice that of a non H-bonded dimer. As in our previous papers, we compare E_{pol}(RVS) to E_{pol} *(SIBFA),

as computed prior to iterating on the induced dipoles, and E_{pol}(VR) to E_{pol} (SIBFA), after completion of the iterations. E_{pol}(VR) is obtained as the difference between ΔE(HF) and E_1(RVS) and E_{ct}(RVS). δE_{nadd}(SIBFA) of -9.2 kcal/mol is close to the δE_{nadd}(QC) of -9.6 kcal/mol. A close agreement is also found regarding polarization and charge-transfer. Thus for E_{pol}(RVS) and E_{pol}*, δE_{nadd} amounts to -5.9 and -5.8 kcal/mol (respectively). It increases in magnitude for both E_{pol}(VR) and E_{pol}(SIBFA), to -8.8 and -8.4 kcal./mol, respectively. Such increases were previously noted as signatures for cooperativity. E_{ct}(RVS) is also clearly cooperative, even though its δE_{nadd} has a lesser magnitude (-0.8 kcal/mol in both QC and SIBFA). Such a result has precedents with the cyclic water pentamers and hexamers [57]. In these complexes, as with GQ, each monomer simultaneously acts as proton acceptor from one neighbor and a proton donor to the other.

Correlated results (Table 2). ΔE_{tot}(SIBFA) amounting to -68.8 kcal/mol has a much closer agreement with ΔE(B97-D3) amounting to -69.8 kcal/mol than with ΔE(B3LYP-D3) amounting to -74.7 kcal/mol. Such closer agreements with the former functional have been previously noted [70, 71]. δE_{nadd} has similar values with both functionals (-11.5 and -11.8 kcal/mol), however δE_{nadd} (SIBFA) is smaller (-8.8 kcal/mol). We have no explanation for this reduction in magnitude of δE_{nadd} (SIBFA) as compared to the situation at the HF level. A larger magnitude for ΔE(DFT) value of -79.1 kcal/mol was recently reported by Paragi and Fonseca Guerra [36] but this was possibly due to the use of different basis set and functional (BLYP-D/TZ2P) and/or stacked geometry.

b). Stacked half-quartets. The results are reported in Table 3 and 4 at HF/RVS and correlated levels, respectively, regarding the four-guanine complex and the six separate dimeric complexes G1-G2 till G1'-G2'.

HF/RVS calculations. ΔE(HF) is overestimated by ΔE(SIBFA) by 4 kcal/mol out of 8. This was unexpected, the more so, as it is due to E_{MTP*} accountable for a 5.8 kcal/mol overestimation, only partly compensated for by the other contributions. Examination of the individual dimers shows the error in E_{MTP*} to originate mainly from the three stacked complexes G1-G2, G2-G1', and G2-G2', namely 1.5 kcal/mol for each. This could again diagnose some shortcoming in the present derivation of the distributed multipoles, more acute in stacked arrangements where the quadrupolar contributions could be more effective than in the H-bonded complexes. Regarding the second-order contributions, we observe δE_{nadd} to now be positive, indicative of anticooperativity. It is slightly more pronounced in SIBFA than in

QC/RVS (2.2 versus 1.7 kcal/mol). It stems predominantly from E_{pol}, nevertheless E_{ct} has a small, yet beyond rounding-off error, contribution to it.

Correlated calculations. ΔE_{tot}(SIBFA) of -38.0 kcal/mol now compares much more favorably to ΔE(B3LYP-D3) and ΔE(B97-D3) of -39.8 and-34.8 kcal/mol, respectively. The agreement is better with the former functional, a reverse situation to the one occurring with the H-bonded complexes. There is a significantly more uniform agreement with the six guanine dimers than was the case at the HF level. This could indicate a better balanced multipolar distribution derived at the DFT than at the HF level. But it is not precluded that the choice of the parameters used in the GDMA procedure was better adapted for the DFT-derived multipoles than those used for the HF ones. δE_{nadd} of 1.5 kcal/mol for SIBFA is closer to δE_{nadd} for B3LYP-D3 (1.6 kcal/mol) than for B97-D3 (2.2 kcal/mol).

In the absence of metal cations, such values of δE_{nadd} are about five times smaller than those found with an opposite sign for each of the two quartets, so that the stacking of two G quartets should be dominated by cooperativity. However it should be noted that there are four equivalent 'half-quartets', G1-G2/G1'-G2' till G4-G1/G4'G1', each one sharing two G bases from the previous one. A complete analysis would need to be done involving all eight bases of the two stacked GQ complexes, with as well as without metal cations. It is planned in future studies. At this stage it was essential to evaluate how well the trends and magnitudes of δE_{nadd} found in QC could be retrieved in SIBFA.

c). Two stacked G quartets (Table 5). The results are fully consistent with those found at the quartet level. At the HF level), ΔE(SIBFA) is larger than ΔE(HF) by an amount nearly twice as large as with one quartet (the BSSE correction was not subtracted). At the correlated level, ΔE_{tot}(SIBFA) of -169.8 kcal/mol is larger in magnitude than ΔE(B97-D3) of -168.6 kcal/mol by 1 kcal/mol out of 169, while it was smaller than it by 1 kcal/mol out of 69 in one quartet. It is smaller in magnitude than ΔE(B3LYP-D3) of -184.0 by 14 kcal/mol out of 180, an amount only slightly larger than the double of the 6 kcal/mol out of 70 found with one quartet. It is noted that the SIBFA and B97-D3 values of -169 kcal/mol are now close to the -172.4 reported by Paragi and Fonseca Guerra for the stacked GQ dimer [36]. It is instructive to compute the amount of stabilization brought by stacking, upon comparing these ΔE_{tot} values to twice the values found in the isolated quartets. Such values amount to -137.6, -139.6, and -149.4 in SIBFA, B97-D3 and B3LYP-D3, respectively. The stacking of the two G quartets

thus results into additional stabilization energies, δ_{stack}, of -36.6, -40.8, and -30.3 kcal/mol in these respective approaches. The close δ_{stack} values found in SIBFA and B97-D3 imply that the additional stabilization brought by stacking and its impact on cooperativity, are computed consistently by these two approaches. It is noteworthy that their difference, 4.2 kcal/mol, is smaller than the B97-D3 and B3LYP-D3 δ_{stack} difference of 10.5 kcal/mol.

We deem these preliminary analyses to be essential prior to studying the cation complexes of the stacked G quartets. With two cations thus ten interacting entities, there is a total of forty-five 'dimer' interactions, namely twenty-eight base-base, sixteen base-cation, and one cation-cation interaction. How well the H-bonded and stacked base-base interactions, modulated by the potentials and fields of the other bases and the cations, are accounted for by APMM methods, can critically impact the potential energy surfaces they generate for the stacked G quartet-cation complexes

2. Channeling of one monovalent cation (Li^+, Na^+, K^+, Rb^+) through two stacked G quartets.

The cation is displaced along the Z axis from bottom to top in fifteen steps of 0.25 Å amplitude. We retain the coordinates adopted by Gkionis et al. [37]. However the atom ordering is not the same. The one used in the SIBFA library of fragments starts with H(9), N9, C8, etc. The G8 complex was reconstructed by molecular graphics to superimpose with the one given by Gkionis et al. With this construction, the planar separation between the two quartets is 3.4 Å, but while each quartet is flat, there can be small deviations from the uniform Z values of -1.7 and +1.7 Å for the bottom and the top quartets. The geometries are given in Supp. Info. The cation starts at Z=-2.72 Å, 1 Å below the center of the bottom quartet, and ends at Z=0.78 Å, 2.5 Å above that center and 0.9 Å below the center of the top quartet. The energy profiles for the channeling of each cation are reported in Figures 2a-d regarding ΔE(HF) and ΔE(SIBFA) computed with HF-derived multipoles and polarizabilities, along with the E_1 and E_2 contributions of ΔE(SIBFA). Figures 3a-e report the corresponding profiles for ΔE(B97-D3) and ΔE_{tot}(SIBFA) now with correlated multipoles and polarizabilities and the dispersion contribution. The fifth point in the plot corresponds to the cation in the plane of the bottom quartet, and twelfth point to the cation at mid-distance from the two quartets. We report in Appendices I and II the Tables giving the energies plotted in Figures 2a-d and 3a-e. We do

not list the separate values of E_{pol} and E_{ct} within E_2. E_{ct} has shallower variations than E_{pol}, and is in the range -15 -- -20 kcal/mol.

a) ΔE(HF) and ΔE(SIBFA) profiles. The four cations display markedly different QC energy profiles, which can be closely matched by SIBFA.

Li$^+$ (Figure 2a) ΔE(HF) has two shallow minima, at Z=-1.47 Å, 0.25 Å above the first quartet, and at Z=0.78 Å, with values of -211.3 and -210.4 kcal/mol, respectively. ΔE(SIBFA) has minima at these two points as well, with values of -209.1 and -207.0 kcal/mol, respectively. Both ΔE(HF) and ΔE(SIBFA) have a shallow maximum at Z=0 Å, when the cation is in-between the two quartets, with values of -206.7 and -202.5 kcal/mol, respectively. In SIBFA, E_1 has a much larger magnitude than E_2, with a ratio in the range 1.4-1.65. However, while it is E_1 that confers its shape to ΔE(SIBFA) in the first half of the trajectory, namely until Z=-1, it is the reverse in the second half, and the shallow maximum at Z=0 Å is clearly due to E_2.

Na+ (Figure 2b). Both ΔE(HF) and ΔE(SIBFA) curves are very shallow in-between Z=-1.22 and Z=0.78 Å, where the energy variations are <1.5 kcal/mol out of 205, i.e. less than 1%. The curves are actually shallower than the corresponding Li^+ curve, despite the larger size of the cation. Two very flat minima can still be discerned. The first is at Z=-0.97 Å (HF) and at Z=-1.22 Å (SIBFA) with ΔE(HF) and ΔE(SIBFA) values of -205.6 and -207.2 kcal/mol, respectively. The second minimum is at Z=0.78, with virtually identical HF and SIBFA values of -206.2 kcal/mol. As was the case with Li^+, the shape of ΔE(SIBFA) is dictated by E_1 in the first half of the trajectory and by E_2 in the second half.

K$^+$ (Figure 2c). The HF and SIBFA energy profiles dramatically differ from the Li^+ and Na^+ ones, and they do so on many counts. There now is one single, well-defined minimum at Z=0, namely when the cation is in the center of the cavity (ΔE(HF)= -196.3 and ΔE(SIBFA)=-195.8 kcal/mol). This is a clear indication for the fact that owing to its size, K^+ is the most suited cation to bridge the two G quartets at equal distances. Along the alkali cation series, it is also the cation endowed with the most favorable stacked G quartet binding affinity as recently demonstrated by QC energy balance analyses [33]. The relative weight of E_1 to E_2 fluctuates much more than with the two smaller cations: from 1.26 in the first third of the curve to 1.74 at, and close to the minimum.

Rb$^+$ (Figure 2d). The HF and SIBFA curves have much more pronounced features than the K^+ curves. Both have a well-defined maximum at Z=-1.72 Å, namely when the cation in the center of the first monomer, a clear indication of the fact that the cation is oversized with

respect to the GQ cavity size. As for K^+, the energy minima are at Z=0 Å, in the center of the cavity, but are deeper than for K^+. ΔE(HF) and ΔE(SIBFA) at the minimum are numerically close (-186.7 and -190.0 kcal/mol, respectively), and this is the case for the entire trajectory, except to a limited extent (up to 4%) in the high-lying zone. The ratios of E_1 to E_2 are now very contrasting. E_1 dictates its shape to the entire trajectory. Except for the first point, it is lesser in magnitude than E_2 until Z=-1.2 Å, and has the least value at Z=-1.72 Å, when the cation is in the center of the first quartet.

b) ΔE(DFT-D3) and ΔE_{tot}(SIBFA) profiles.

We will mostly display the results found with the B97-D3 functional, which in keeping with previous results was the one giving rise to the closest agreements with ΔE_{tot}(SIBFA) [67, 68]. The ΔE(B3LYP-D3) curves, shown below for the Li^+ complexes, are invariably parallel to the B97-D3 one but app. 30 kcal/mol lower. The increases in magnitude upon passing from ΔE(HF) to ΔE(B97-D3) and from ΔE(SIBFA) to ΔE_{tot}(SIBFA), are closely similar for all four cations. E_{disp}(SIBFA) stems solely from the guanine-guanine interactions contributing -88.5 kcal/mol for all complexes. It is not shown in the figures.

Li^+ (Figure 3a). While ΔE_{tot}(SIBFA) has the same shallow profile as ΔE(SIBFA) with a flat minimum at Z=-1.22 Å. ΔE(B97-D3) undergoes a regular decrease until Z= -0.47 Å. The decrease then becomes more accented with a minimum at Z=0.03 Å, and this is observed as well for ΔE(B3LYP-D3) but had not happened with ΔE(HF). This appears to stem from the D3 functional. Thus Figure 3b recasts the profile computed with the B3LYP functional in the absence of such correction, seen to parallel ΔE(HF), but not ΔE(B3LYP-D3).

Na^+ (Figure 3c). ΔE(B97-D3) has a profile similar to the Li^+ one, with its minimum at Z=0.03, while ΔE_{tot}(SIBFA) has a shallow behavior from Z=-1.7 Å throughout, with two shallow minima at Z=-1.22 Å and Z=0.78 Å. As a result, the relative error of ΔE_{tot}(SIBFA) with respect to ΔE(B97-D3) is the smallest at Z=-1.72 Å, at the center of the first quartet (2%), and is the largest at Z= 0 Å (6%).

K^+ (Figure 3d). ΔE(B97-D3) and ΔE_{tot}(SIBFA) have similar shapes, as in the absence of correlation/dispersion (Figure 2c). There is a shallow increase in magnitude in the region Z= -2.72 till -0.97 Å, followed by a more accented descent to the minimum at Z=0 Å. As with Na^+, the minimum is deeper for ΔE(B97-D3) than for ΔE_{tot}(SIBFA), and the relative error is the largest there (4%) while it was <1% at the HF level.

Rb^+ (Figure 3e). ΔE(B97-D3) and ΔE_{tot}(SIBFA) have more parallel shapes than was the case with the smaller cations, the offset never exceeding 11.3 kcal/mol ouf of 220, its average value being of 7.3 kcal/mol, the average energy difference amounting to 3%. As with the HF calculation, the maximum of both ΔE(B97-D3) and ΔE_{tot}(SIBFA) is at -1.72 Å in the center of the first quartet, and the minimum is at Z=0.0.

3. Channeling of two monovalent cations (Li^+, Na^+, K^+, Rb^+) through two stacked G quartets.

We report in Appendices III and IV the Tables giving the energies plotted in Figures 4a-d and 5a-d. We do not list the separate values of E_{pol} and E_{ct} within E_2. E_{ct} has shallower variations than E_{pol}, and is in the range -18 -- -24 kcal/mol.

a) ΔE(HF) and ΔE(SIBFA) profiles.

The results are reported in Figures 4a-d. For all cations, both QC and SIBFA profiles very significantly differ from the corresponding one-cation profiles.

Li+ (Figure 4a). The minima of both QC and SIBFA are shifted from Z=-1.47 to Z=-1.72 Å, namely in the center of the first quartet, after which the energy raises continuously rather than plateauing. The E_1/E_2 ratio decreases progressively, until E_2 becomes larger in magnitude at Z=-0.22 Å. This clearly translates the raise in total polarization energy of the two G quartets upon shortening the cation-cation distance, counteracting the raise in their mutual Coulomb repulsion. It is notable that the sum of E_1 and E_2 enables SIBFA to match ΔE(HF) with relative errors < 2% thus accounting for the Z-dependent ΔE magnitude increase upon passing from the one- to the two-cation G8 complexes.

Na^+ (Figure 4b). The profiles of ΔE(HF) and ΔE(SIBFA) both resemble the Li^+ ones, with a minimum shifted at Z=-1.72 Å, a continuous raise thereafter, and a E_1/E_2 crossing at Z=-0.22. In the low-energy zone, ΔE(SIBFA) matches ΔE(HF) with relative errors of 2%, comparable to those found with Li^+, but now overestimates it rather than underestimating it.

K^+ (Figure 4c). The Z=0 Å minimum has disappeared owing to the increased electrostatic repulsion undergone by the moving cation. Instead, the energy plateaus along the whole Z=-2.72 -- -0.22 Å region, undergoing <2% variations. Except for the first two points, E_2 is now larger in magnitude than E_1, the gap increasing steeply past Z=0 Å. The relative error of ΔE(SIBFA) with respect to ΔE(HF) is 3%.

Rb^+ (Figure 4d). With respect to the K^+ curve, a shallow maximum is present at Z=-1.72 Å, when the moving cation is in the center of the first quartet, and there still does exist a minimum at Z=-0.47 Å, 0.5 Å before the center of the cavity is reached. Past this minimum, the energy raises more steeply than with K^+, owing to the much larger short-range Rb^+-Rb^+ than K^+-K^+ short-range repulsion. Thus with both QC and SIBFA there are two well-defined minima, at the start of the trajectory (Z=-2.72 Å) and close to the center of the cavity (Z=-0.47 Å). E_2 is now invariably larger in magnitude than E_1, but the shape of ΔE is dictated by E_1. The relative errors of ΔE(SIBFA) are larger than in the two K^+ case, and can reach 6% in the low-energy zone.

b) ΔE(B97-D3) and ΔE_{tot}(SIBFA) profiles.

Li+ (Figure 5a). Both QC and SIBFA curves closely resemble their counterparts at the HF level (Figure 4a). There is a shallow minimum at Z=-1.72 Å, in the center of the first quartet followed by a progressive rise in the energy. The E_1 and E_2 curves cross at Z=-0.72 Å, 0.30 Å earlier than at the HF level. The relative SIBFA versus QC error now averages 5%, larger than the 2% error found at the HF level.

Na^+ (Figure 5b). Again, the shapes of ΔE(B97-D3) and ΔE_{tot}(SIBFA) are very similar to their HF counterparts. The shallow minimum in the first half of the trajectory locates Na^+ at Z=-1.47 Å, namely 0.25 Å above the center of the first quartet, and the E_1/E_2 crossing occurs 0.5 Å earlier than at the HF level. The relative SIBFA error averages 3% over the relevant energy zone but is lowest at the minimum.

K^+ (Figure 5c). Both curves plateau closely similar to their HF counterparts. There is a discernible minimum for Z=-0.72 Å, and the total energies start to rise steeply as the moving cation progresses 0.5 Å past it and beyond. The crossing of the E_1/E_2 curves now occurs at the very start of the trajectory, rather than 0.5 Å past it as with the HF curves. The relative errors in SIBFA are strikingly small (1%) over the low energy range of distances, namely in thirteen points covering a 3 Å trajectory.

Rb^+ (Figure 5d). As with the HF curves, a local maximum is located in the center of the first quartet, and for both SIBFA and QC the global minimum occurs at Z =--0.47 Å, 0.5 Å before the center of the cavity. E_2 has larger magnitudes than E_1 throughout and the gap increases along the entire trajectory except close to the energy minimum. The relative errors in SIBFA are <2% for the thirteen first points in the trajectory.

Non-Covalent Interaction (NCI) analyses. Analyzing the sign of the second eigenvalues, λ_2, of the electron density Hessian matrix shows the nature of the non-covalent interaction:

attractive if λ_2 is negative, and repulsive if positive. If ρ denotes the electronic density, a plot of the reduced gradient density, s, as a function of the product $\lambda_2\rho$ provides information on such a nature, classified as attractive, weak, or repulsive.

A red-green-blue color scheme is chosen for the 2D and 3D plots to distinguish between strong and attractive interactions such as ionic or hydrogen bonds (in blue), weak interactions such as van der Waals or related interactions (in green), and repulsive interactions (in red).

We first consider the two stacked quartets prior to cation binding (Figure 6). The onset of stabilizing inter-quartet interactions is attested by the large, deep-green isosurfaces in the mid-plane (Figures 6a-b). Within each quartet plane, the spherical blue-green isosurfaces between H(N1) and O6, and between H(N2) and N7, attest to the onset of strong inter-molecular H-bonds. The red oval surfaces in the middle of both rings of each guanine attest to local intra-molecular repulsions (Figure 6a).

We next consider the NCI plots for one K^+ cation channeling along the Z axis (Figures 7a-d). When it is located beneath the first quartet (Z=-2.7 Å, Figure 7a), the K^+ -- O6 interactions are translated by downward-pointing green disk-shaped isosurfaces, with no visible perturbation of the mid-plane isosurfaces. Its in-plane location (Z=-1.7 Å, Figure 7b) translates by in-plane alignments of O6, K^+, and the disk-shaped isosurfaces, with little impact on the mid-plane isosurfaces. The location of K+ in the center of the cavity (Z=0.0 Å, Figure 7c) translates, on the one hand, by an upward displacement of the disk isosurfaces connecting K^+ to the bottom quartet O6 and downward displacement of the disk isosurfaces connecting it to the top quartet O6. The mid-plane isosurfaces are less disjoint than with Z=-2.7 and -1.7 Å, or in the absence of cation altogether. When K^+ is closer to the top quartet (Z=0.7 Å, Figure 7d), the O6-K^+ isosurfaces stemming from the bottom quartet have faded out, while those stemming from the top quarter have their density increased. The mid-plane isosurfaces are not significantly impacted.

The NCI features along the four steps of this trajectory become more accented in the presence of an additional cation held on top of the top quartet at Z=2.8 Å (Figures 8a-d). Whatever the location of the channeling cation, there are four upward directed disk-shaped isosurfaces between the four O6 atoms of the top quartet and the topmost cation. As was the case with one K^+, the corresponding four isosurfaces of the bottom quartet follow the moving cation: downward-pointing for Z=-2.8 Å (8a), in-plane location for Z=-1.8 Å (8b), upward-pointing for Z=0.0 Å (8c), and fading out for Z=0.8 Å (8d). For Z=0.0 Å, it is instructive to observe that each O6 atom from the top quartet contributes two disk-shaped isosurfaces: upward-

pointing toward the top K^+, and downward-pointing toward the central K^+. The mid-plane isosurfaces are brighter than the corresponding ones with only one K^+.

The different peaks present in the 2D plot can be analyzed for a better understanding of the features of the 3D isosurfaces. We can detect first the signature peak of the guanines, prior to K^+ binding (Figure 6c). There is a neat peak in the attractive region ($\lambda_2\rho$ =-0.02 au). It corresponds to the inter-molecular H1-O6 and H2-N7 bonds. The two green peaks ($\lambda_2\rho$ = -0.005 and 0.0 au) correspond to the mid-plane isosurfaces. The red peak at $\lambda_2\rho$=0.025 au corresponds to the repulsive intra-ring interactions in each guanine.

We next consider the evolutions of these peaks in the presence of one and two K^+ cations. When K^+ is below the bottom quartet (Z=-2.8 Å, Figure 7a), an additional blue peak appears at $\lambda_2\rho$ =-0.015 au. When K^+ is in the center of this quartet (Z=-1.8 Å, Figure 8b), the peak is shifted to a more attractive region with $\lambda_2\rho$ =-0.03 au. When K^+ moves to the center of the cavity (Z=0.0 Å, Figure 7c), or closer to the topmost quartet (Z=-0.8 A, Figure 7d), this blue peak disappears. For the first two points (Z=-2.8 and -1.8 Å) and for the last one (Z=+0.8 Å, Figure 7d), the two central green peaks on both sides of $\lambda_2\rho$ =0 have the same features as in the absence of K^+. When K^+ is in the center of the cavity (Z=0.0 Å), the left-most peak becomes wider, consistent with the increase of the mid-point isosurfaces in the 3D plots (Figure 7c).

We next consider the two K^+ complexes. There are no marked differences for the first two points (Z=-2.8 and -1.8 Å, Figures 8a-b) with respect to the one-cation case. When K^+ is in the center of the cavity, on the other hand, both left and right green peaks around $\lambda_2\rho$= 0.0 au are enlarged with respect to the one-cation case. At Z=0.8 Å, an additional red peak appears at $\lambda_2\rho$ =0.015 au. It translates the onset of short-range repulsive interactions between the two cations which are at 2.0 Å from one another.

For both Na^+ and Rb^+ complexes, both 2D and 3D plots present very similar features as with K^+ (not shown). The most conspicuous feature which differentiates between them is found with the two-cation complexes at Z=0.7 Å. It relates to the repulsive peak at $\lambda_2\rho$ = 0.015 au, more spread-out with Rb^+ than with K^+, and virtually undetectable with Na^+.

In conclusion, the NCI analysis demonstrates that both the guanine-guanine and guanine-metal key interactions are in a van der Waals regime. The strength of guanine-metal interactions clearly depends on the cation position, being maximized when the metal is located at the center of the cavity. The relative selectivity of the various cations therefore

relies on subtle variations of van der Waals interactions that can be highlighted by the presented supermolecular interaction energies.

Discussion.

We have carried out benchmark comparisons of the SIBFA APMM procedure against QC results in a demanding test case, the complex of two stacked guanine quartets (GQ) with one or two alkali cations Li^+, Na^+, K^+ and Rb^+, and the energy profile for the channeling of one cation along the Z axis with or without another one set above the topmost quartet. These tests are motivated by the emerging importance of GQs in molecular biology, in drug design, and in nanoscience. The alkali cations K^+ and Na^+ inside their cavity can play a major role in their stabilization. Stacked GQ's in a wealth of settings clearly constitute a privileged avenue for a manifold of future large-scale APMM applications. They are stabilized by the simultaneous interplay of multiply H-bonded interactions, stacking interactions between extended and polar surfaces, and cation-ligand interactions. Non-additivity effects strongly come into play, and have to be correctly quantified by APMM procedures. It is thus mandatory to objectively benchmark their expectable accuracy against high-level QC, and how well they perform compared to non-polarizable potentials [37]. We have adopted a staged approach comparing first ΔE(SIBFA) to ΔE(HF) and then ΔE_{tot}(SIBFA) to ΔE(DFT-D3). An essential motivation for this is the fact that all ΔE(SIBFA) parameters were derived beforehand on the basis of RVS EDA's done at the HF level with the aug-cc-pVTZ(-f) level [59], then extended to alkali cations [40] and to cytosine and guanine [41]. The passage to correlated tests is done solely upon replacing the HF-derived multipoles and polarizabilities by those derived at the DFT level, and adding an appropriately rescaled E_{disp} contribution. Can we, then, be equally successful, if at all, in reproducing in succession both HF and DFT-D calculations?

We considered the stabilization energies of one, then of two stacked quartets prior to cation binding, and then the complexes of two stacked GQ's with one and with two cations.

-*In-plane G quartet*. At the HF level, in each of the four doubly H-bonded dimers G1-G2 till G4-G1, E_{MTP} and E_{rep} were each accountable for overestimations of 0.5 kcal/mol out of 16 (E_C) and 11 (E_{exch}). This indicates that improvements to E_{MTP} could be sought for, such as GEM or ISA. These could impact $E_{rep,}$ as well, since E_{rep} embodies a dependence upon electrostatics in its prefactor. The second-order contributions, E_{pol} and E_{ct} gave close matches to their QC counterparts. Cooperativity was correctly accounted for, δE_{nadd} amounting to -9.6 and to -9.2 kcal/mol in HF and SIBFA, respectively. At the correlated level, ΔE_{tot}(SIBFA) of -

68.8 kcal/mol was found to have a closer agreement to ΔE(B97-D3) of -69.8 kcal/mole than to ΔE(B3LYP-D3) of -74.7.

-*Two stacked half-quartets*. Such an arrangement involves a doubly H-bonded dimer of the first quartet and one of the two most overlapping H-bonded dimers of the other quartet. δE_{nadd} now has a positive sign, indicative of local anticooperativity, and its QC value is satisfactorily accounted for in SIBFA: 1.5 vs. 2.2 kcal/mol at the HF level, and 1.5 versus 1.6 and 2.2 kcal/mol at the B3LYP-D3 and 2.2 levels, respectively. As with the in-plane G quartet, better agreements are found between ΔE_{tot}(SIBFA) and ΔE(DFT-D3) than at the HF level. Thus ΔE_{tot}(SIBFA) amounts to -38.0 kcal/mol as compared to -39.8 and -34.8 kcal/mol with the B3LYP-D3 and B97-D3 functionals.

-*Two-stacked GQ complex*. The best agreement was between ΔE_{tot}(SIBFA) and ΔE(B97-D3), namely -169.8 vs. -168.6 kcal/mol. This value is smaller than the -184 kcal/mol ΔE(B3LYP-D3) one. The agreement between SIBFA and B97-D3 is again closer than that of the two DFT-D3 procedures between themselves. This was observed previously in a Zn(II)-metalloprotein recognition site [68], and is also found in all mono- and dication curves.

-*Cation channeling*. We next compared the ΔE(SIBFA) and ΔE(HF) profiles for one cation channeling in the absence of the other. SIBFA could closely match the QC profiles for all four cations, the relative ΔE error being always <2% in the low-energy zones. Li^+ and Na^+ had similar, very flat profile, nevertheless two minima were discernible for both: the first, about 0.50 Å above the center of the first quartet, and the second, at the end of the trajectory. A flat maximum was at the center of the cavity, found by both QC and SIBFA. In SIBFA, the magnitude of ΔE was mostly due to E_1 accounting for its two thirds, yet it was E_2 that conferred to ΔE its shape in the last part of the trajectory. K^+ had a starkly different profile, increasing regularly in magnitude until it reached the center of the cavity. The E_1/E_2 ratio was much more strongly variable than with the two cations, from 1.25 till 1.80 in the center of the cavity. The contrasted E_1 and E_2 profiles from Z=-1.47 Å and beyond are noteworthy, yet they sum up to confer the right profile to ΔE(SIBFA) as compared to ΔE(HF). A significant reshape of the energy profile, imposed by E_1, occurred with Rb^+, with an accented maximum in the center of the first quartet, and a minimum in the center of the cavity.

There are lesser agreements upon comparing ΔE_{tot}(SIBFA) and ΔE(B97-D3) for the two lighter cations, Li^+ and Na^+. ΔE(B97-D3) and ΔE(B3LYP-D3) contrary to ΔE(HF) now have a minimum at Z=0 Å. It is not found for ΔE_{tot}(SIBFA), which behaves exactly as ΔE(HF) and

ΔE(SIBFA), but also as ΔE(B3LYP). The reasons for the different B3LYP and B3LYP-D3 shapes remain to be clarified. ΔE_{tot}(SIBFA) compares much more favorably to ΔE(B97-D3) with K^+, the Z=0 Å minimum at the center of the cavity being the 'natural' one. Nevertheless the relative SIBFA error is still the largest at this point: 4% as compared to 2% in the first half of the trajectory. There is a more regular SIBFA/QC parallelism with Rb^+, the relative error being contained to <3% throughout.

The energy profiles in the presence of a second cation are markedly different. Could, upon decreasing the cation-cation distance, the increase of magnitude of E_2 due to increased polarization correctly compensate for the decrease of E_1 magnitude due to increased cation-cation electrostatic repulsion, and also, for the larger cations close to the end of their trajectory, the increase of their short-range repulsion? Any E_2/E_1 imbalance, that could be further magnified by the non-additivities of E_{pol} and E_{ct} in the presence of the second cation, could severely downgrade the SIBFA versus QC parallelism. Regarding ΔE(SIBFA) and ΔE(HF), the lighter two cations had closely similar energy profiles, their minima now occurring in the center of the first quartet, rather than above it. The relative error is for both <2% over the whole low-energy zone. A cross-over of the E_1 and E_2 curves occurs at 0.25 Å before reaching the center of the cavity. A close parallelism is also found for K^+. With both QC and SIBFA, the energy minimum is considerably shallower than in the one-cation case, and is displaced 0.75 Å beneath the center of the cavity. The E_1/E_2 crossover now occurs already at 0.5 Å after the start of the trajectory. The relative SIBFA/QC error is < 3% in the low-energy range. The shape of the K^+ energy profile is further accented with Rb^+. While the first maximum is still in the center of the first quartet, the minimum is displaced 0.5 Å beneath the center of the cavity. E_2 is larger in magnitude throughout the entire trajectory, the gap increasing upon Rb^+ progression along the Z axis. ΔE(SIBFA) very closely reproduces ΔE(HF) in the first part of the trajectory, the relative error being <2%, increasing slowly to 5% at the energy minimum. Closely similar conclusions can be reached regarding ΔE(B97-D3) and ΔE_{tot}(SIBFA). For both Li^+ and Na^+, the two curves display good parallelism, with relative SIBFA errors < 4% (Li^+) and <3% (Na^+). The energy minima are in the center of the first quartet. The E_1/E_2 crossover occurs for ΔE_{tot}(SIBFA) 0.50 Å earlier than for ΔE(SIBFA), translating the larger relative weight of E_2 with respect to E_1 with correlated multipoles and polarizabilities. For K^+ and Rb^+, there is a rather remarkable overlap of the SIBFA and QC trajectories throughout. The relative errors are now 1%. Nevertheless the fact that we recover a better agreement with two than with one cation implies there are some compensations of

errors that we will seek to unravel in future work. The E_1/E_2 crossover now occurs at the very start of the trajectories. For K^+, the energy minimum is at Z=-0.72 Å, consistent with its ΔE(HF) location. For Rb^+, with both ΔE(B97-D3) and ΔE_{tot}(SIBFA), it is shifted 0.25 Å upward compared to K^+, and is more accented.

The present results could be used to benchmark other polarizable potentials [69-72] or semi-empirical QC methods. For this purpose we give as Supp. Info S1-S4 the G09 input data used for the G8 complexes with two cations. The moving cation is given its coordinates at the start of the trajectory (Z=-2.72 Å), the Z coordinate of the fixed cation being set at 2.80 Å.

Concluding remarks.

The present SIBFA benchmarks appear convincing and should lend credence to prospective simulations of stacked G quartets and their metal cation complexes. Long-duration molecular dynamics (MD) on periodic GQ stacks and their complexes with metal cations are thus envisaged. They will benefit from the recent integration of the SIBFA potential and its gradients into the massively parallel Tinker-HP package [73]. This should enable to study their ion transport properties, the impact of molecular environment in different phases, such as liquid, gel, solid, or close to a conducting surface, etc. MD could also provide poses for post-processing by QC to calculate their most salient electronic properties. GQs could be connected together by variable linkers, to yield supramolecular complexes of tunable properties. We are also pursuing the refinements of the SIBFA potential. On the one hand, alternatives to GDMA multipoles are being tested. On the other hand, in line with our previous work [41], additional SAPT calculations [74-76] on the complexes of nucleic acid bases with cation and water probes are being performed. This should enable a finer-tuning, now at the correlated level, of each of the five SIBFA contributions against its QC counterpart. There are simultaneous ongoing SIBFA refinements of the sugar-phosphate backbone of DNA and RNA which should pave the way for future APMM simulations of quadruplex DNA and their ligand complexes. These will be reported subsequently.

Appendices 1-4. Channeling of one cation (Li^+- Rb^+) along the Z axis of two stacked G4 tetramers. Comparison of ΔE(QC) and ΔE(SIBFA) values. Consistent with Figures 2-5, the Z values (first column) are multiplied by a factor of 100 for clarity.

Appendix 1. Channeling of one cation along the Z axis of two stacked G4 tetramers. Comparison of ΔE(HF) and ΔE(SIBFA) values (in kcal/mol).

	Li^+		Na^+		K^+		Rb^+	
	ΔE(HF)	ΔE(SIBFA)	ΔE(HF)	ΔE(SIBFA)	ΔE(HF)	ΔE(SIBFA)	ΔE(HF)	ΔE(SIBFA)
-272	-187.94	-185.48	-184.18	-184.91	-170.95	-172.78	-156.73	-159.00
-247	-195.25	-192.88	-190.14	-191.72	-172.08	-174.75	-153.32	-153.96
-222	-201.51	-199.33	-195.1	-197.52	-172.13	-175.69	-149.11	-147.52
-197	-206.37	-204.36	-198.99	-202.01	-172.32	-176.44	-146.02	-142.35
-172	-209.64	-207.64	-201.88	-205.09	-173.65	-177.92	-146.02	-141.33
-147	-211.32	-209.12	-203.90	-206.78	-176.68	-180.65	-149.63	-145.87
-122	-211.13	-208.98	-205.12	-207.2	-181.11	-184.39	-157.34	-155.02
-97	-210.78	-207.68	-205.61	-206.61	-186.02	-188.34	-166.25	-166.16
-72	-209.49	-205.81	-205.52	-205.39	-190.44	-191.71	-174.77	-176.47
-47	-207.95	-203.99	-205.13	-204.06	-193.74	-194.08	-181.43	-184.17
-22	-206.94	-202.77	-204.75	-203.11	-195.71	-195.4	-185.48	-188.66
3	-206.69	-202.49	-204.68	-202.9	-196.30	-195.83	-186.67	-189.95
28	-207.32	-203.24	-205.03	-203.53	-195.55	-195.42	-184.97	-188.09
53	-208.67	-204.88	-205.64	-204.84	-193.45	-194.1	-180.46	-183.03
78	-210.36	-207.00	-206.20	-206.43	-190.10	-191.73	-173.50	-174.83

Appendix 2.

Channeling of one cation along the Z axis of two stacked G4 tetramers. Comparison of ΔE(ΔE(B97-D3) and ΔE(SIBFA) values (in kcal/mol).

	Li^+		Na^+		K^+		Rb^+	
	ΔE(QC)	ΔE_{tot}(SIBFA)	ΔE(QC)	ΔE_{tot}(SIBFA)	ΔE(QC)	ΔE_{tot}(SIBFA)	ΔE(QC)	ΔE_{tot}(SIBFA
-272	-271.74	-256.79	-265.75	-255.82	-250.46	-243.78	-232.92	-230.18
-247	-276.48	-264.35	-270.44	-262.68	-250.82	-245.82	-231.08	-225.29
-222	-281.91	-270.94	-274.47	-268.51	-250.45	-246.84	-226.75	-219
-197	-286.17	-276.10	-277.8	-273.07	-250.48	-247.68	-223.98	-213.99
-172	-289.17	-279.56	-280.57	-276.30	-252.05	-249.33	-224.43	-213.15
-147	-291.05	-281.25	-283.02	-278.23	-255.67	-252.29	-229.10	-217.9
-122	-291.93	-281.37	-285.21	-278.98	-261.08	-256.33	-237.11	-227.31
-97	-292.05	-280.35	-287.12	-278.78	-267.37	-260.65	-247.40	-238.73
-72	-292.21	-278.78	-288.94	-277.98	-273.23	-264.4	-256.94	-249.35
-47	-295.15	-277.29	-290.76	-277.07	-277.7	-267.16	-264.26	-257.39
-22	-300.27	-276.41	-292.14	-276.53	-280.09	-268.87	-268.93	-262.23
3	-301.07	-276.50	-292.61	-276.71	-280.73	-269.68	-270.46	-263.89
28	-299.39	-277.65	-292.07	-277.70	-279.85	-269.64	-268.25	-262.42
53	-294.47	-279.69	-290.71	-279.33	-277.15	-268.66	-260.92	-257.73
78	-292.62	-282.20	-289.04	-281.20	-272.93	-266.59	-255.41	-249.91

Appendix 3.

Channeling of one cation along the Z axis of two stacked G4 tetramers in the presence of a fixed cation above the top tetramer. Comparison of ΔE(HF) and ΔE(SIBFA) values (in kcal/mol).

	Li^+		Na^+		K^+		Rb^+	
	ΔE(HF)	ΔE(SIBFA)	ΔE(HF)	ΔE(SIBFA)	ΔE(HF)	ΔE(SIBFA)	ΔE(HF)	ΔE(SIBFA)
-272	-239.74	-234.17	-232.48	-233.21	-207.03	-210.38	-179.99	-184.88
-247	-245.78	-240.49	-237.13	-238.94	-206.66	-211.25	-175.07	-178.75
-222	-250.63	-245.73	-240.61	-243.5	-205.2	-210.97	-169.2	-171.08
-197	-253.88	-249.37	-242.82	-246.58	-203.62	-210.31	-164.27	-164.52
-172	-255.28	-251.03	-243.76	-248.01	-202.98	-210.15	-162.17	-161.87
-147	-254.73	-250.57	-243.46	-247.74	-203.74	-210.94	-163.76	-164.47
-122	-252.33	-248.13	-241.93	-245.84	-205.47	-212.34	-168.26	-171.28
-97	-248.34	-244.08	-239.15	-242.47	-206.97	-213.48	-173.71	-179.51
-72	-243.13	-238.90	-235.17	-237.92	-207.61	-213.38	-177.75	-186.08
-47	-237.10	-233.09	-230.15	-232.55	-205.56	-211.32	-178.36	-188.59
-22	-230.54	-226.99	-224.38	-226.65	-200.92	-206.67	-173.45	-184.99
3	-223.50	-220.64	-216.86	-220.25	-192.23	-198.13	-159.44	-171.71
28	-215.63	-213.67	-208.18	-212.94	-176.75	-182.29	-128.61	-139.43
53	-206.14	-205.23	-196.98	-203.75	-147.18	-149.92	-63.27	-63.05
78	-193.62	-193.85	-181.06	-190.95	-85.05	-75.84	75.55	126.08

Appendix 4.

Channeling of one cation along the Z axis of two stacked G4 tetramers in the presence of a fixed cation above the top tetramer. Comparison of ΔE(B97-D3) and ΔE_{tot}(SIBFA) values (in kcal/mol).

	Li^+		Na^+		K^+		Rb^+	
	ΔE(QC)	ΔE_{tot}(SIBFA)	ΔE(QC)	ΔE_{tot}(SIBFA)	ΔE(QC)	ΔE_{tot}(SIBFA)	ΔE(QC)	ΔE_{tot}(SIBFA
-272	-327.72	-309.20	-317.50	-307.44	-288.21	-284.77	-259.11	-259.59
-247	-332.32	-315.79	-321.04	-313.30	-287.36	-285.81	-253.71	-253.69
-222	-336.50	-321.28	-323.81	-318.00	-285.65	-285.69	-247.81	-246.26
-197	-339.33	-325.19	-325.72	-321.26	-284.13	-285.24	-243.16	-239.96
-172	-340.66	-327.17	-326.85	-322.97	-283.81	-285.36	-241.43	-237.61
-147	-340.58	-327.11	-327.32	-323.09	-285.12	-286.53	-243.54	-240.58
-122	-338.98	-325.13	-327.02	-321.69	-287.71	-288.41	-248.87	-247.80
-97	-335.82	-321.58	-325.79	-318.89	-290.62	-290.09	-255.40	-256.49
-72	-331.35	-316.92	-323.73	-314.93	-292.47	-290.54	-260.86	-263.54
-47	-326.14	-311.64	-320.85	-310.14	-292.27	-289.03	-262.92	-266.54
-22	-320.40	-306.06	-316.51	-304.74	-288.85	-284.86	-259.13	-263.39
3	-313.96	-300.22	-309.96	-298.75	-280.67	-276.73	-246.18	-250.49
28	-306.29	-293.73	-300.67	-291.74	-265.66	-261.19	-216.46	-218.52
53	-296.61	-285.70	-288.15	-282.72	-237.32	-228.99	-153.92	-142.35
78	-283.64	-274.66	-269.87	-269.97	-178.80	-154.97	-21.58	46.69

Supporting Information available for publication.

G09 input data used for the G8 complexes with two cations (Li^+, Na^+, K^+, or Rb^+). The moving cation is given its coordinates at the start of the trajectory (Z=-2.72 Å) the Z coordinate of the fixed cation being set at 2.80 Å.

Acknowledgments.

We wish to thank the Grand Equipement National de Calcul Intensif (GENCI), Institut du Développement et des Ressources en Informatique Scientifique (IDRIS), Centre Informatique de l'Enseignement Supérieur (CINES, France, project No. x2009-075009), and the Centre de Ressources Informatiques de Haute Normandie (CRIHAN, Rouen, France, project 1998053). JES and JS acknowledge support by the Czech Science Foundation [grant number 16-13721S]. Their research has also been financially supported by the Ministry of Education, Youth and Sports of the Czech Republic under the project CEITEC 2020 (LQ1601).

References.

1. Rhodes, D.; Lipps, H. J., G-Quadruplexes and their Regulatory Roles in Biology. *Nucleic Acids Research* **2015,** *43* (18), 8627-8637.
2. Williamson, J. R., G-Quartet Structures in Telomeric DNA. *Annual Review of Biophysics and Biomolecular Structure* **1994,** *23* (1), 703-730.
3. Rodriguez, R.; Miller, K. M.; Forment, J. V.; Bradshaw, C. R.; Nikan, M.; Britton, S.; Oelschlaegel, T.; Xhemalce, B.; Balasubramanian, S.; Jackson, S. P., Small Molecule-Induced DNA Damage Identifies Alternative DNA Structures in Human Genes. *Nature chemical biology* **2012,** *8* (3), 301-310.
4. Biffi, G.; Tannahill, D.; McCafferty, J.; Balasubramanian, S., Quantitative Visualization of DNA G-Quadruplex Structures in Human Cells. *Nature chemistry* **2013,** *5* (3), 182-186.
5. Siddiqui-Jain, A.; Grand, C. L.; Bearss, D. J.; Hurley, L. H., Direct Evidence for a G-Quadruplex in a Promoter Region and its Targeting with a Small Molecule to Repress c-*Myc* Transcription. *Proceedings of the National Academy of Sciences of the United States of America* **2002,** *99* (18), 11593-11598.
6. Dexheimer, T. S.; Sun, D.; Hurley, L. H., Deconvoluting the Structural and Drug-Recognition Complexity of the G-Quadruplex-Forming Region Upstream of the bcl-2 P1 Promoter. *Journal of the American Chemical Society* **2006,** *128* (16), 5404-5415.
7. Wei, D.; Parkinson, G. N.; Reszka, A. P.; Neidle, S., Crystal Structure of a c-*Kit* Promoter Quadruplex Reveals the Structural Role of Metal Ions and Water Molecules in Maintaining Loop Conformation. *Nucleic Acids Research* **2012,** *40* (10), 4691-4700.
8. Agrawal, P.; Hatzakis, E.; Guo, K.; Carver, M.; Yang, D., Solution Structure of the Major G-Quadruplex Formed in the Human VEGF Promoter in K(+): Insights into Loop

Interactions of the Parallel G-Quadruplexes. *Nucleic Acids Research* **2013,** *41* (22), 10584-10592.
9. Métifiot, M.; Amrane, S.; Litvak, S.; Andreola, M.-L., G-Quadruplexes in Viruses: Function and Potential Therapeutic Applications. *Nucleic Acids Research* **2014,** *42* (20), 12352-12366.
10. Amrane, S.; Kerkour, A.; Bedrat, A.; Vialet, B.; Andreola, M.-L.; Mergny, J.-L., Topology of a DNA G-Quadruplex Structure Formed in the HIV-1 Promoter: A Potential Target for Anti-HIV Drug Development. *Journal of the American Chemical Society* **2014,** *136* (14), 5249-5252.
11. Alcaro, S.; Musetti, C.; Distinto, S.; Casatti, M.; Zagotto, G.; Artese, A.; Parrotta, L.; Moraca, F.; Costa, G.; Ortuso, F.; Maccioni, E.; Sissi, C., Identification and Characterization of New DNA G-Quadruplex Binders Selected by a Combination of Ligand and Structure-Based Virtual Screening Approaches. *Journal of Medicinal Chemistry* **2013,** *56* (3), 843-855.
12. Teulade-Fichou, M.-P.; Carrasco, C.; Guittat, L.; Bailly, C.; Alberti, P.; Mergny, J.-L.; David, A.; Lehn, J.-M.; Wilson, W. D., Selective Recognition of G-Quadruplex Telomeric DNA by a Bis(quinacridine) Macrocycle. *Journal of the American Chemical Society* **2003,** *125* (16), 4732-4740.
13. Castor, K. J.; Liu, Z.; Fakhoury, J.; Hancock, M. A.; Mittermaier, A.; Moitessier, N.; Sleiman, H. F., A Platinum(II) Phenylphenanthroimidazole with an Extended Side-Chain Exhibits Slow Dissociation from a c-Kit G-Quadruplex Motif. *Chemistry. A European Journal* **2013,** *19* (52), 17836-17845.
14. Balasubramanian, S.; Hurley, L. H.; Neidle, S., Targeting G-Quadruplexes in Gene Promoters: a Novel Anticancer Strategy? *Nature reviews. Drug discovery* **2011,** *10* (4), 261-275.
15. Rajendran, A.; Endo, M.; Hidaka, K.; Teulade-Fichou, M.-P.; Mergny, J.-L.; Sugiyama, H., Small Molecule Binding to a G-Hairpin and a G-Triplex: a New Insight into Anticancer Drug Design Targeting G-Rich Regions. *Chemical Communications* **2015,** *51* (44), 9181-9184.
16. Livshits, G. I.; Stern, A.; Rotem, D.; Borovok, N.; Eidelshtein, G.; Migliore, A.; Penzo, E.; Wind, S. J.; Di Felice, R.; Skourtis, S. S. et al. Long-Range Charge Transport in Single G-Quadruplex DNA Molecules. *Nat Nano* **2014,** *9* (12), 1040-1046.
17. Ma'ani Hessari, N.; Spindler, L.; Troha, T.; Lam, W.-C.; Drevenšek-Olenik, I.; Webba da Silva, M., Programmed Self-Assembly of a Quadruplex DNA Nanowire. *Chemistry. A European Journal* **2014,** *20* (13), 3626-3630.
18. Jissy, A. K.; Ashik, U. P. M.; Datta, A., Nucleic Acid G-Quartets: Insights into Diverse Patterns and Optical Properties. *The Journal of Physical Chemistry C* **2011,** *115* (25), 12530-12546.
19. Hua, Y.; Changenet-Barret, P.; Improta, R.; Vayá, I.; Gustavsson, T.; Kotlyar, A. B.; Zikich, D.; Šket, P.; Plavec, J.; Markovitsi, D., Cation Effect on the Electronic Excited States of Guanine Nanostructures Studied by Time-Resolved Fluorescence Spectroscopy. *The Journal of Physical Chemistry C* **2012,** *116* (27), 14682-14689.
20. Liu, S.-P.; Weisbrod, S. H.; Tang, Z.; Marx, A.; Scheer, E.; Erbe, A., Direct Measurement of Electrical Transport Through G-Quadruplex DNA with Mechanically Controllable Break Junction Electrodes. *Angewandte Chemie International Edition* **2010,** *49* (19), 3313-3316.
21. Trajkovski, M.; Plavec, J., Assessing Roles of Cations in G-Quadruplex-Based Nanowires by NMR. *The Journal of Physical Chemistry C* **2012,** *116* (44), 23821-23825.
22. Parkinson, G. N.; Lee, M. P. H.; Neidle, S., Crystal Structure of Parallel Quadruplexes from Human Telomeric DNA. *Nature* **2002,** *417* (6891), 876-880.

23. Bouaziz, S.; Kettani, A.; Patel, D. J., A K Cation-Induced Conformational Switch within a Loop Spanning Segment of a DNA Quadruplex Containing G-G-G-C Repeats. *Journal of Molecular Biology* **1998,** *282* (3), 637-652.
24. Lim, K. W.; Amrane, S.; Bouaziz, S.; Xu, W.; Mu, Y.; Patel, D. J.; Luu, K. N.; Phan, A. T., Structure of the Human Telomere in K(+) Solution: a Stable Basket-Type G-Quadruplex with only two G-Tetrad Layers. *Journal of the American Chemical Society* **2009,** *131* (12), 4301-4309.
25. Campbell, N. H.; Parkinson, G. N.; Reszka, A. P.; Neidle, S., Structural Basis of DNA Quadruplex Recognition by an Acridine Drug. *Journal of the American Chemical Society* **2008,** *130* (21), 6722-6724.
26. Agrawal, P.; Lin, C.; Mathad, R. I.; Carver, M.; Yang, D., The Major G-Quadruplex Formed in the Human BCL-2 Proximal Promoter Adopts a Parallel Structure with a 13-nt Loop in K(+) Solution. *Journal of the American Chemical Society* **2014,** *136* (5), 1750-1753.
27. Ren, J.; Qu, X.; Trent, J. O.; Chaires, J. B., Tiny Telomere DNA. *Nucleic Acids Research* **2002,** *30* (11), 2307-2315.
28. Fadrná, E.; Špačková, N. a.; Sarzyñska, J.; Koča, J.; Orozco, M.; Cheatham, T. E.; Kulinski, T.; Šponer, J., Single Stranded Loops of Quadruplex DNA As Key Benchmark for Testing Nucleic Acids Force Fields. *Journal of Chemical Theory and Computation* **2009,** *5* (9), 2514-2530.
29. Islam, B.; Stadlbauer, P.; Krepl, M.; Koca, J.; Neidle, S.; Haider, S.; Sponer, J., Extended Molecular Dynamics of a *c-kit* Promoter Quadruplex. *Nucleic Acids Research* **2015,** *43* (18), 8673-8693.
30. Stadlbauer, P.; Mazzanti, L.; Cragnolini, T.; Wales, D. J.; Derreumaux, P.; Pasquali, S.; Šponer, J., Coarse-Grained Simulations Complemented by Atomistic Molecular Dynamics Provide New Insights into Folding and Unfolding of Human Telomeric G-Quadruplexes. *Journal of Chemical Theory and Computation* **2016,** *12* (12), 6077-6097.
31. Šponer, J.; Bussi, G.; Stadlbauer, P.; Kührová, P.; Banáš, P.; Islam, B.; Haider, S.; Neidle, S.; Otyepka, M., Folding of Guanine Quadruplex Molecules–Funnel-Like Mechanism or Kinetic Partitioning? An Overview from MD Simulation Studies. *Biochimica et Biophysica Acta (BBA) - General Subjects, in press*. http://dx.doi.org/10.1016/j.bbagen.2016.12.008
32. Bazzi, S.; Novotný, J.; Yurenko, Y. P.; Marek, R., Designing a New Class of Bases for Nucleic Acid Quadruplexes and Quadruplex-Active Ligands. *Chemistry. A European Journal* **2015,** *21* (26), 9414-9425.
33. Zaccaria, F.; Paragi, G.; Fonseca Guerra, C., The Role of Alkali Metal Cations in the Stabilization of Guanine Quadruplexes: why K+ is the Best. *Physical Chemistry Chemical Physics* **2016,** *18* (31), 20895-20904.
34. Šponer, J.; Mládek, A.; Špačková, N.; Cang, X.; Cheatham, T. E.; Grimme, S., Relative Stability of Different DNA Guanine Quadruplex Stem Topologies Derived Using Large-Scale Quantum-Chemical Computations. *Journal of the American Chemical Society* **2013,** *135* (26), 9785-9796.
35. Fonseca-Guerra, C.; Zijlstra, H.; Paragi, G.; Bickelhaupt, F. M., Telomere Structure and Stability: Covalency in Hydrogen Bonds, Not Resonance Assistance, Causes Cooperativity in Guanine Quartets. *Chemistry – A European Journal* **2011,** *17* (45), 12612-12622.
36. Paragi, G.; Fonseca-Guerra, C., Cooperativity in the Self-Assembly of the Guanine Nucleobase into Quartet and Ribbon Structures on Surfaces. *Chemistry – A European Journal* **2017***, 23*, (13) 3042-3050.
37. Gkionis, K.; Kruse, H.; Platts, J. A.; Mládek, A.; Koča, J.; Šponer, J., Ion Binding to Quadruplex DNA Stems. Comparison of MM and QM Descriptions Reveals Sizable

Polarization Effects Not Included in Contemporary Simulations. *Journal of Chemical Theory and Computation* **2014,** *10* (3), 1326-1340.
38. Gresh, N.; Šponer, J. E.; Špačková, N. a.; Leszczynski, J.; Šponer, J., Theoretical Study of Binding of Hydrated Zn(II) and Mg(II) Cations to 5'-Guanosine Monophosphate. Toward Polarizable Molecular Mechanics for DNA and RNA. *The Journal of Physical Chemistry B* **2003,** *107* (33), 8669-8681.
39. Gresh, N.; Cisneros, G. A.; Darden, T. A.; Piquemal, J.-P., Anisotropic, Polarizable Molecular Mechanics Studies of Inter- and Intramolecular Interactions and Ligand−Macromolecule Complexes. A Bottom-Up Strategy. *Journal of Chemical Theory and Computation* **2007,** *3* (6), 1960-1986.
40. Dudev, T.; Devereux, M.; Meuwly, M.; Lim, C.; Piquemal, J.-P.; Gresh, N., Quantum-Chemistry Based Calibration of the Alkali Metal Cation Series (Li+-Cs+) for Large-Scale Polarizable Molecular Mechanics/Dynamics Simulations. *Journal of Computational Chemistry* **2015,** *36* (5), 285-302.
41. Gresh, N.; Sponer, J. E.; Devereux, M.; Gkionis, K.; de Courcy, B.; Piquemal, J.-P.; Sponer, J., Stacked and H-Bonded Cytosine Dimers. Analysis of the Intermolecular Interaction Energies by Parallel Quantum Chemistry and Polarizable Molecular Mechanics. *The Journal of Physical Chemistry B* **2015,** *119* (30), 9477-9495.
42. Gresh, N.; Pullman, B. A Theoretical study of the Selective Entrapment of Alkali and Ammonium Cations Between Guanine Tetramers. Int. J. Quantum Chem. Quantum Biol. Symp. **1986**, *12*, 49-56.
43. Dunning, Jr., T. H. D., Gaussian Basis Sets for Use in Correlated Molecular Calculations. I. The atoms boron through neon and hydrogen. *The Journal of Chemical Physics* **1989,** *90* (2), 1007-1023.
44. Feller, D., The Role of Data Bases in Support of Computational Chemistry Calculations. *Journal of Computational Chemistry* **1996,** *17* (13), 1571-1586.
45. Machado, S. F.; Camiletti, G. G.; Neto, A. C.; Jorge, F. E.; Jorge, R. S., Gaussian Basis Set of Triple Zeta Valence Quality for the Atoms from K to Kr: Application in DFT and CCSD(T) Calculations of Molecular Properties. *Molecular Physics* **2009,** *107* (16), 1713-1727.
46. Bergner, A.; Dolg, M.; Küchle, W.; Stoll, H.; Preuß, H., Ab Initio Energy-Adjusted Pseudopotentials for Elements of Groups 13–17. *Molecular Physics* **1993,** *80* (6), 1431-1441.
47. Stevens, W. J.; Fink, W. H., Frozen Fragment Reduced Variational Space Analysis of Hydrogen Bonding Interactions. Application to the Water Dimer. *Chemical Physics Letters* **1987,** *139* (1), 15-22.
48. Schmidt, M. W.; Baldridge, K. K.; Boatz, J. A.; Elbert, S. T.; Gordon, M. S.; Jensen, J. H.; Koseki, S.; Matsunaga, N.; Nguyen, K. A.; Su, S.; Windus, T. L.; Dupuis, M.; Montgomery, J. A., General Atomic and Molecular Electronic Structure System. *Journal of Computational Chemistry* **1993,** *14* (11), 1347-1363.
49. Grimme, S.; Antony, J.; Ehrlich, S.; Krieg, H., A Consistent and Accurate Ab Initio Parametrization of Density Functional Dispersion Correction (DFT-D) for the 94 Elements H-Pu. *The Journal of Chemical Physics* **2010,** *132* (15), 154104.
50. Lee, C.; Yang, W.; Parr, R. G., Development of the Colle-Salvetti Correlation-Energy Formula into a Functional of the Electron Density. *Physical Review B* **1988,** *37* (2), 785-789.
51. Becke, A. D., A New Mixing of Hartree–Fock and Local Density-Functional Theories. *The Journal of Chemical Physics* **1993,** *98* (2), 1372-1377.
52. Frisch, M. J.; Trucks, G. W.; Schlegel, H. B.; Scuseria, G. E.; Robb, M. A.; Cheeseman, J. R.; Scalmani, G.; Barone, V.; Mennucci, B.; Petersson, G. A.et al. Gaussian 09, Revision B.01 Wallingford CT, 2009.

53. Stone, A. J., Distributed Multipole Analysis: Stability for Large Basis Sets. *Journal of Chemical Theory and Computation* **2005,** *1* (6), 1128-1132.
54. Piquemal, J.-P.; Gresh, N.; Giessner-Prettre, C., Improved Formulas for the Calculation of the Electrostatic Contribution to the Intermolecular Interaction Energy from Multipolar Expansion of the Electronic Distribution. *The Journal of Physical Chemistry A* **2003,** *107* (48), 10353-10359.
55. Piquemal, J.-P.; Chevreau, H.; Gresh, N., Toward a Separate Reproduction of the Contributions to the Hartree−Fock and DFT Intermolecular Interaction Energies by Polarizable Molecular Mechanics with the SIBFA Potential. *Journal of Chemical Theory and Computation* **2007,** *3* (3), 824-837.
56. Garmer, D. R.; Stevens, W. J., Transferability of Molecular Distributed Polarizabilities from a Simple Localized Orbital Based Method. *The Journal of Physical Chemistry* **1989,** *93* (25), 8263-8270.
57. Gresh, N., Model, Multiply Hydrogen-Bonded Water Oligomers (N = 3−20). How Closely Can a Separable, ab Initio-Grounded Molecular Mechanics Procedure Reproduce the Results of Supermolecule Quantum Chemical Computations? *The Journal of Physical Chemistry A* **1997,** *101* (46), 8680-8694.
58. Creuzet, S.; Gresh, N.; Langlet, J. Adjustment of the SIBFA Method for Potential Maps to Study Hydrogen Bonding Vibrational Frequencies. *J. Chim.-Phys.,* **1991***, 88*, 2399-2409.
59. Devereux, M.; Gresh, N.; Piquemal, J.-P.; Meuwly, M., A Supervised Fitting Approach to Force Field Parametrization with Application to the SIBFA Polarizable Force Field. *Journal of Computational Chemistry* **2014,** *35* (21), 1577-1591.
60. Law, M. M.; Hutson, J. M., I-NoLLS: A Program for Interactive Nonlinear Least-Squares Fitting of the Parameters of Physical Models. *Computer Physics Communications* **1997,** *102* (1–3), 252-268.
61. Johnson, E. R.; Keinan, S.; Mori-Sánchez, P.; Contreras-García, J.; Cohen, A. J.; Yang, W., Revealing Non-Covalent Interactions. *Journal of the American Chemical Society* **2010,** *132* (18), 6498-6506.
62. Contreras-García, J.; Johnson, E. R.; Keinan, S.; Chaudret, R.; Piquemal, J.-P.; Beratan, D. N.; Yang, W., NCIPLOT: a program for plotting non-covalent interaction regions. *Journal of chemical theory and computation* **2011,** *7* (3), 625-632.
63. Misquitta, A. J.; Stone, A. J.; Fazeli, F., Distributed Multipoles from a Robust Basis-Space Implementation of the Iterated Stockholder Atoms Procedure. *Journal of Chemical Theory and Computation* **2014,** *10* (12), 5405-5418.
64. Lillestolen, T. C.; Wheatley, R. J., Atomic Charge Densities Generated Using an Iterative Stockholder Procedure. *The Journal of Chemical Physics* **2009,** *131* (14), 144101.
65. Elking, D. M.; Cisneros, G. A.; Piquemal, J.-P.; Darden, T. A.; Pedersen, L. G., Gaussian Multipole Model (GMM). *Journal of Chemical Theory and Computation* **2010,** *6* (1), 190-202.
66. Cisneros, G. A., Application of Gaussian Electrostatic Model (GEM) Distributed Multipoles in the AMOEBA Force Field. *Journal of Chemical Theory and Computation* **2012,** *8* (12), 5072-5080.
67. El Hage, K.; Piquemal, J.-P.; Hobaika, Z.; Maroun, R. G.; Gresh, N., Substituent-Modulated Affinities of Halobenzene Derivatives to the HIV-1 Integrase Recognition Site. Analyses of the Interaction Energies by Parallel Quantum Chemical and Polarizable Molecular Mechanics. *The Journal of Physical Chemistry A* **2014,** *118* (41), 9772-9782.
68. Gresh, N.; Perahia, D.; de Courcy, B.; Foret, J.; Roux, C.; El-Khoury, L.; Piquemal, J.-P.; Salmon, L., Complexes of a Zn-Metalloenzyme Binding Site with Hydroxamate-Containing Ligands. A Case for Detailed Benchmarkings of Polarizable Molecular

Mechanics/Dynamics Potentials when the Experimental Binding Structure is Unknown. *Journal of Computational Chemistry* **2016,** *37* (32), 2770-2782.
69. Ponder, J. W.; Wu, C.; Ren, P.; Pande, V. S.; Chodera, J. D.; Schnieders, M. J.; Haque, I.; Mobley, D. L.; Lambrecht, D. S.; DiStasio, R. A. et al. Current Status of the AMOEBA Polarizable Force Field. *The Journal of Physical Chemistry B* **2010,** *114* (8), 2549-2564.
70. Zhang, C.; Bell, D.; Harger, M.; Ren, P., Polarizable Multipole-Based Force Field for Aromatic Molecules and Nucleobases. *Journal of Chemical Theory and Computation* **2017,** *13,* 666-676.
71. Lemkul, J. A.; MacKerell, A. D., Balancing the Interactions of Mg2+ in Aqueous Solution and with Nucleic Acid Moieties For a Polarizable Force Field Based on the Classical Drude Oscillator Model. *The Journal of Physical Chemistry B* **2016,** *120* (44), 11436-11448.
72. Harder, E.; Anisimov, V. M.; Vorobyov, I. V.; Lopes, P. E. M.; Noskov, S. Y.; MacKerell, A. D.; Roux, B., Atomic Level Anisotropy in the Electrostatic Modeling of Lone Pairs for a Polarizable Force Field Based on the Classical Drude Oscillator. *Journal of Chemical Theory and Computation* **2006,** *2* (6), 1587-1597.
73. Tinker HP_Team, Tinker-HP, http://www.ip2ct.upmc.fr/tinkerHP, 2016. Accessed March 29, 2017.
74. Jansen, G.; Hesselmann, A., Comment on "Using Kohn−Sham Orbitals in Symmetry-Adapted Perturbation Theory To Investigate Intermolecular Interactions". *The Journal of Physical Chemistry A* **2001,** *105* (49), 11156-11157.
75. Jeziorski, B.; Moszynski, R.; Szalewicz, K., Perturbation Theory Approach to Intermolecular Potential Energy Surfaces of van der Waals Complexes. *Chemical Reviews* **1994,** *94* (7), 1887-1930.
76. Misquitta, A. J.; Jeziorski, B.; Szalewicz, K., Dispersion Energy from Density-Functional Theory Description of Monomers. *Physical Review Letters* **2003,** *91* (3), 033201.

Figures captions:

Figure 1. Complex of two stacked G quartets with two monovalent cations. Representation of the trajectory followed by the moving cation**.** The fixed cation is located on top of the upper quartet.

Figures 2. Complex of two stacked G quartets with one monovalent cation. ΔE(HF), ΔE(SIBFA), and E_1/E_2(SIBFA) profiles for cation channeling along the Z axis.

2a: Li^+; 2b: Na^+; 2c: K^+; 2d: Rb^+.

Figures 3. Complex of two stacked G quartets with one monovalent cation.

3a: ΔE(B97-D3), ΔE(B3LYP-D3), ΔE_{tot}(SIBFA) and E_1/E_2(SIBFA) profiles for Li^+ channeling along the Z axis.

3b: ΔE(HF), ΔE(B3LYP) and ΔE(SIBFA) profiles for Li^+ channeling.

3c-3d: ΔE(B97-D3), ΔE(B3LYP-D3), ΔE_{tot}(SIBFA) and E_1/E_2(SIBFA) profiles for cation channeling along the Z axis.

3c : Na^+ ; 3d : K^+ ; 3e: Rb^+.

Figure 4. Complex of two stacked G quartets with two monovalent cations with one moving cation. ΔE(HF), ΔE(SIBFA), and E_1/E_2(SIBFA) profiles for cation channeling along the Z axis.

4a: Li^+; 4b: Na^+; 4c: K^+; 4d: Rb^+.

Figure 5. Complex of two stacked G quartets with two monovalent cations with one moving cation. ΔE(B97-D3), ΔE_{tot}(SIBFA), and E_1/E_2(SIBFA) profiles for cation channeling along the Z axis.

5a: Li^+; 5b: Na^+; 5c: K^+; 5d: Rb^+.

Figures 6a-b. 3D plot NCI analysis of the two guanine quartets without cation: (a) in the XZ plane; (b) in the XY plane; and (c) corresponding 2D plot. In the 3D plots, the NCI surfaces correspond to s = 0.50 isosurfaces.

Figures 7a-d. 2D and 3D plot NCI analyses of the two guanine quartets with K^+ along the Z axis: (a): Z = -2.7 Å, (b): Z = -1.7 Å, (c): Z = 0.0 Å, (d): Z = 0.8 Å. In the 3D plots, the NCI surfaces correspond to s = 0.50 isosurfaces.

Figures 8a-d. 2D and 3D plot NCI analyses of the two guanine quartets with a fixed K^+ cation at Z = 2.8 Å and a mobile K^+ cation along the Z axis : (a): Z = -2.7 Å, (b): Z = -1.7 Å, (c): Z= 0.0 Å, (d): Z= 0.8 Å. In the 3D plots, the NCI surfaces correspond to s = 0.50 isosurfaces.

Table 1. Intermolecular interaction energies (kcal/mol) and their contributions in a G4 tetramer and evaluation of non-additivities. Comparisons between ΔE(RVS) and ΔE(SIBFA).

G4 tetramer	QC	SIBFA
E_c/E_{MTP}	-65.8	-67.9
E_{exch}/E_{rep}	44.2	42.4
E_1	-21.7	-25.5
$E_{pol}(RVS)/E_{pol}$*	-17.5	-17.0
$E_{pol}(VR)/E_{pol}$	-23.8	-21.8
E_{ct}	-8.1	-9.2
E_{ct}*	-6.5	
ΔE	-52.0	-56.5

Dimers G1-2, G1-4, G2-3, G3-4	QC	SIBFA
E_c/E_{MTP}	-15.8	-16.4
E_{exch}/E_{rep}	11.1	10.6
E_1	-4.7	-5.8
$E_{pol}(RVS)/E_{pol}$*	-2.9	-2.8
$E_{pol}(VR)/E_{pol}$	-3.7	-3.3
E_{ct}	-1.8	-2.2
E_{ct}*	-1.5	
ΔE	-9.9	-11.3

Dimers G1-3, G2-4	QC	SIBFA
E_c/E_{MTP}	-1.3	-1.3
E_{exch}/E_{rep}	0.0	0.0
E_1	-1.3	-1.3
$E_{pol}(RVS)/E_{pol}$*	-0.1	-0.1
$E_{pol}(VR)/E_{pol}$	-0.1	-0.1
E_{ct}	0.0	0.0
E_{ct}*	0.0	
Summed values.		
E_c/E_{MTP}	-65.8	-67.8
Ee_{xch}/E_{rep}	44.4	42.4
E_1	-21.4	-25.5
$E_{pol}(RVS)/E_{pol}$*	-11.6	-11.4
δE_{nadd}	-5.9	-5.8
$E_{pol}(VR)/Epol$	-15	-13.4
δE_{nadd}	-8.8	-8.4
E_{ct}	-7.3	-8.8
δE_{nadd}	-0.8	-0.8

Table 2. Intermolecular interaction energies (kcal/mol) and their contributions in a G4 tetramer and evaluation of non-additivities. Comparisons between ΔE(DFT-D3) and ΔE_{tot}(SIBFA).

B3LYP-D3

G4 tetramer	QC	SIBFA
ΔE	-74.7	-68.8
ΔE(MP2)	-73.0	
Dimers	QC	SIBFA
G1-2, G1-4, G2-3, G3-4	-15.1	-14.3
G1-3, G2-4	-1.4	-1.4
Summed values	-63.2	-60.0
δE_{nadd}	-11.5	-8.8

B97-D3

G4 tetramer	QC	SIBFA
ΔE	-69.8	-68.8
Dimers	QC	SIBFA
G1-2, G1-4, G2-3, G3-4	-13.8	-14.3
G1-3, G2-4	-1.4	-1.4
Summed values	-58.0	-60.0
δE_{nadd}	-11.8	-8.8

Table 3. Intermolecular interaction energies (kcal/mol) and their contributions in a stacked complex of bases G1-2 and G1'-2' of the first and second G4 tetramers and evaluation of non-additivities. Comparisons between ΔE(RVS) and ΔE(SIBFA).

G4 tetramer	QC	SIBFA
E_c/E_{MTP}	-26.4	-32.0
E_{exch}/E_{rep}	30.4	31.5
E_1	4.0	-0.5
$E_{pol}(RVS)/E_{pol}$*	-6.4	-6.0
$E_{pol}(VR)/E_{pol}$	-9.4	-6.7
E_{ct}	-4.8	-4.6
E_{ct}*	-2.5	
ΔE	-7.8	-11.8

Dimers	QC	SIBFA
G1-G2, G1'-G2'		
E_c/E_{MTP}	-15.8	-16.4
E_{exch}/E_{rep}	11.1	10.7
E_1	-4.7	-5.7
$E_{pol}(RVS)/E_{pol}$*	-2.9	-2.7
$E_{pol}(VR)/E_{pol}$	-3.8	-3.3
E_{ct}	-1.8	-2.2
E_{ct}*	-1.4	
ΔE	-9.9	-11.2
G1-G1'		
E_C/E_{MTP}	-1.3	-1.3
E_{exch}/E_{rep}	0.0	0.0
E_1	-1.3	-1.3
$E_{pol}(RVS)/E_{pol}$*	-0.1	-0.1
$E_{pol}(VR)/E_{pol}$	-0.1	-0.1

E_{ct}	0.0	0.0
E_{ct}*	0.0	
ΔE	-1.4	-1.3
G1-G2'		
E_c/E_{MTP}	2.0	0.5
E_{exch}/E_{rep}	3.0	3.6
E_1	5.0	4.1
$E_{pol}(RVS)/E_{pol}$*	-0.6	-0.7
$E_{pol}(VR)/E_{pol}$	-0.6	-0.7
E_{ct}	-0.5	-0.2
E_{ct}*	-0.1	
ΔE	3.9	3.2
G2-G1'		
E_c/E_{MTP}	2.0	0.4
E_{exch}/E_{rep}	3.1	3.7
E_1	5.1	4.1
$E_{pol}(RVS)/E_{pol}$*	-0.6	-0.7
$E_{pol}(VR)/E_{pol}$	-0.6	-0.7
E_{ct}	-0.4	-0.2
E_{ct}*	-0.1	
ΔE	4.0	3.2
G2-G2'		
E_c/E_{MTP}	2.5	1.0
E_{exch}/E_{rep}	2.3	2.9
E_1	4.8	3.9
$E_{pol}(RVS)/E_{pol}$*	-0.6	-0.6
$E_{pol}(VR)/E_{pol}$	-0.6	-0.6
E_{ct}	-0.2	-0.1
E_{ct}*	-0.1	

ΔE	3.8	3.2
Summed dimer interactions	QC	SIBFA
E_c/E_{MTP}	-26.5	-32.0
E_{exch}/E_{rep}	30.6	31.5
E_1	4.1	-0.5
$E_{pol}(RVS)/E_{pol}$*	-7.7	-7.7
δE_{nadd}	1.3	1.7
$E_{pol}(VR)/E_{pol}$	-9.5	-8.7
δE_{nadd}	1.3	2.0
E_{ct}	-5.1	-4.8
δE_{nadd}	0.3	0.2
E_{ct}*	-3.1	
δE_{nadd}	0.6	0.2
ΔE	-9.5	-14.0
δE_{nadd}	1.7	2.2

Table 4. Intermolecular interaction energies (kcal/mol) and their contributions in a stacked complex of bases G1-2 and G1'-2' of the first and second G4 tetramers and evaluation of non-additivities. Comparisons between ΔE(DFT-D3) and ΔE_{tot}(SIBFA).

B3LYP-D3

G4 tetramer	QC	SIBFA
ΔE	-39.8	-38.0
Dimers	QC	SIBFA
G1-G2	-15.2	-14.3
G1-G1'	-1.3	-1.3
G1-G2'	-3.6	-3.3
G2-G1'	-3.4	-3.3
G2-G2'	-3.1	-3.0
G1'-G2'	-14.9	-14.3
Summed values	-41.4	-39.5
δE_{nadd}	1.6	1.5

B97-D3

G4 tetramer	QC	SIBFA
ΔE	-34.8	-38.0
Dimers	QC	SIBFA
G1-G2	-13.8	-14.3
G1-G1'	-1.2	-1.3
G1-G2'	-3.1	-3.3
G2-G1'	-2.8	-3.3
G2-G2'	-2.5	-3.0
G1'-G2'	-13.5	-14.3
Summed values	-37.0	-39.5
δE_{nadd}	2.2	1.5

Table 5. Intermolecular interaction energies (kcal/mol) in two stacked G4 tetramers.

	QC(HF)	SIBFA	
ΔE	-89.5	-94.8	
	QC(B3LYP-D3)	QC(B97-D3)	ΔE_{tot}(SIBFA)
ΔE	-184.0	-168.6	-169.8

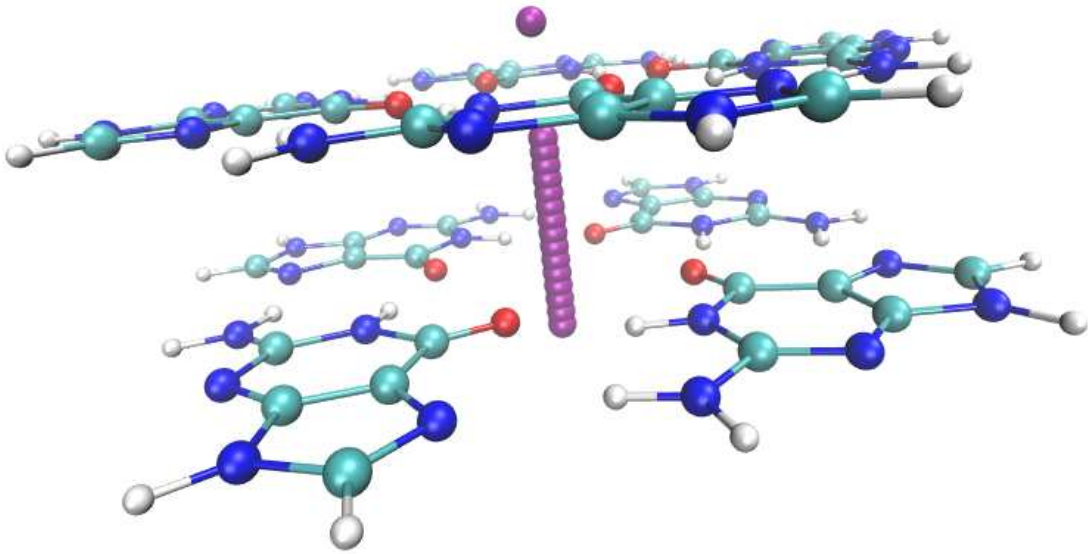

Figure 1. Representation of the complex of two stacked guanine quartets with one monovalent cation channeling along the Z axis and a fixed cation set on top of the upper quartet.

(a)

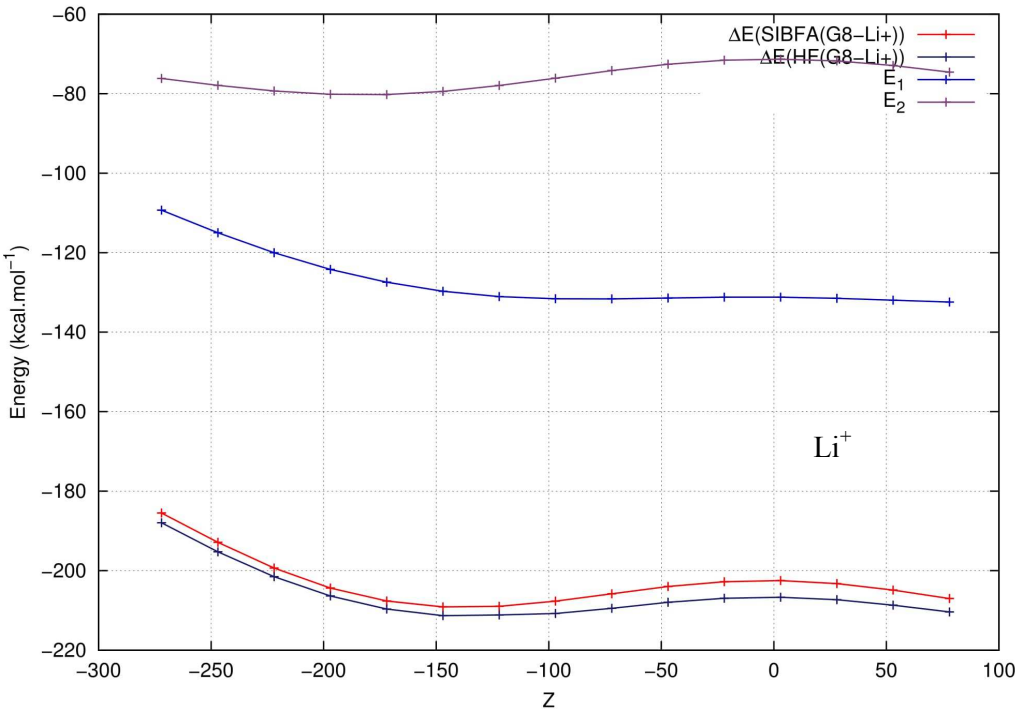
ΔE(SIBFA(G8–Li+))
ΔE(HF(G8–Li+))
E1
E2
Li+
Energy (kcal.mol−1)
Z
−60
−80
−100
−120
−140
−160
−180
−200
−220
−300
−250
−200
−150
−100
−50
0
50
100

(b)

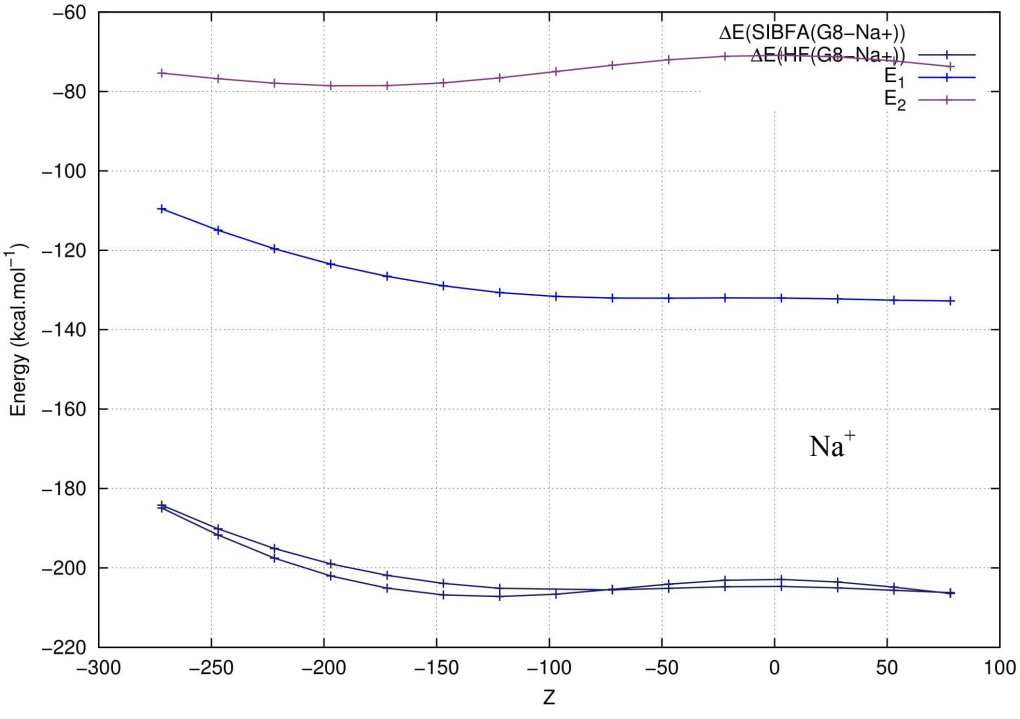
ΔE(SIBFA(G8–Na+))
ΔE(HF(G8–Na+))
E1
E2
Na+
Energy (kcal.mol−1)
Z
−60
−80
−100
−120
−140
−160
−180
−200
−220
−300
−250
−200
−150
−100
−50
0
50
100

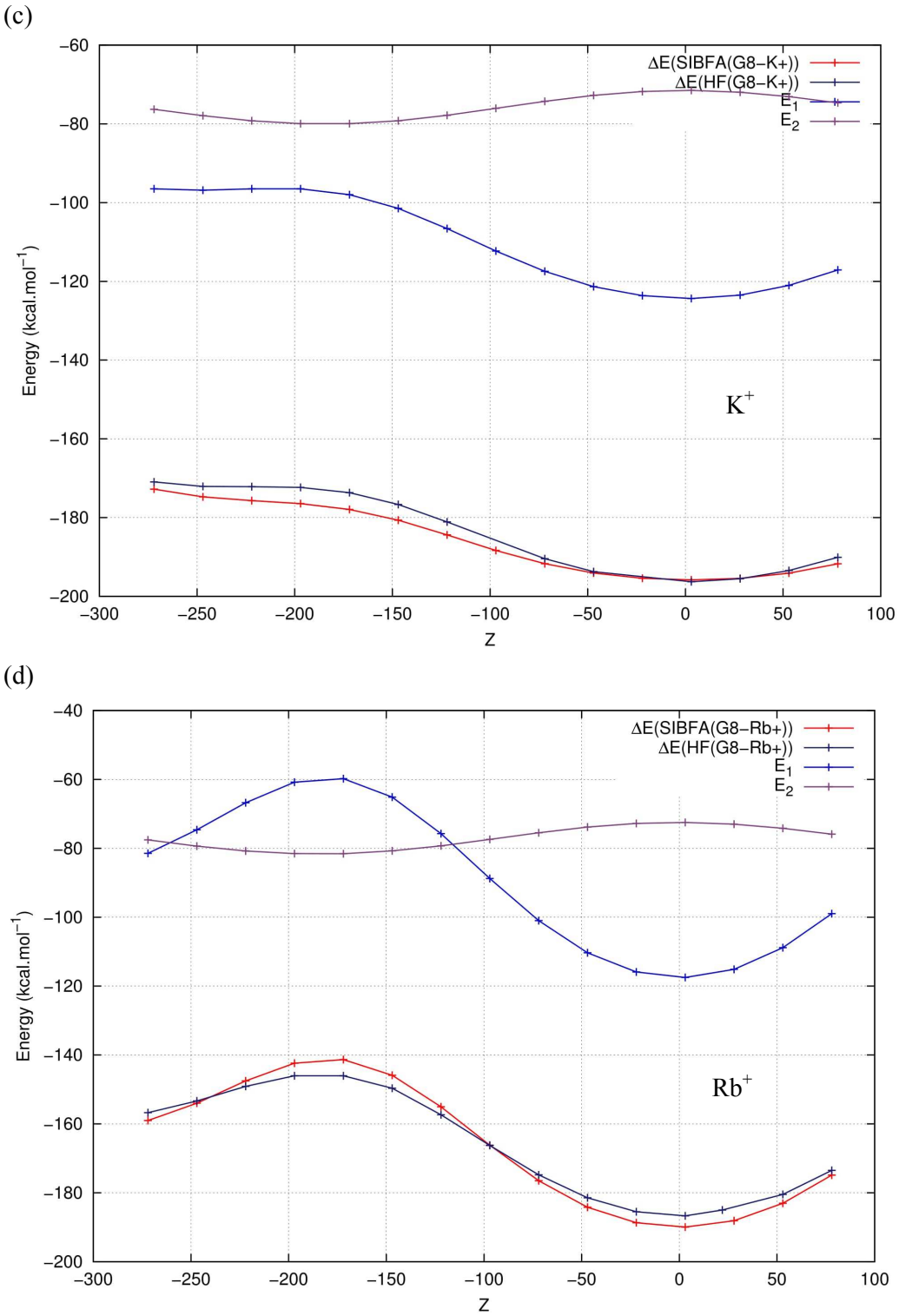

Figure 2. Complex of two stacked G quartets with one monovalent cation. ΔE(HF), ΔE(SIBFA), and E_1/E_2(SIBFA) profiles for cation channeling along the Z axis. 2a: Li^+; 2b:

Na^+; 2c: K^+; 2d: Rb^+. For clarity, the Z values along the abscissa (Å) were multiplied by a factor 100.

(a)

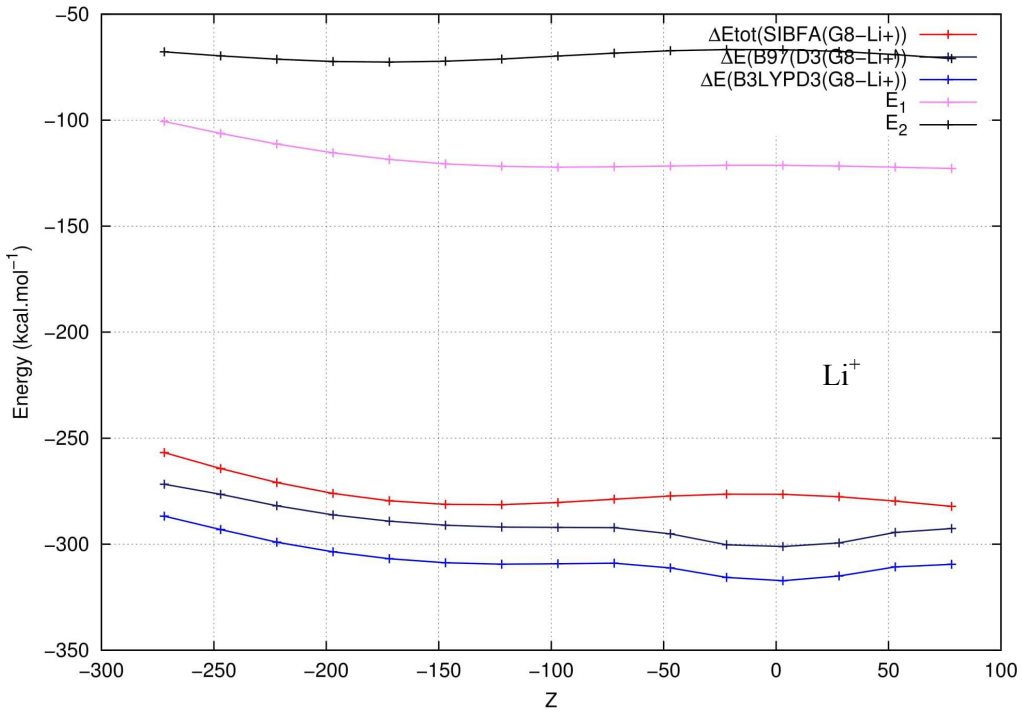

(b)

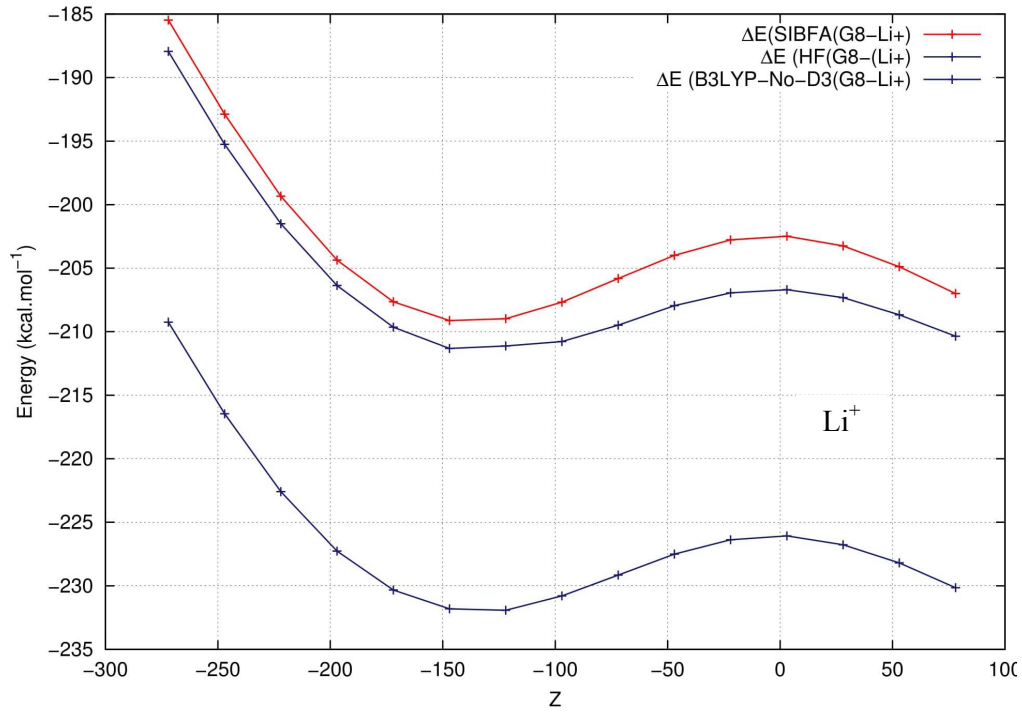

(c)

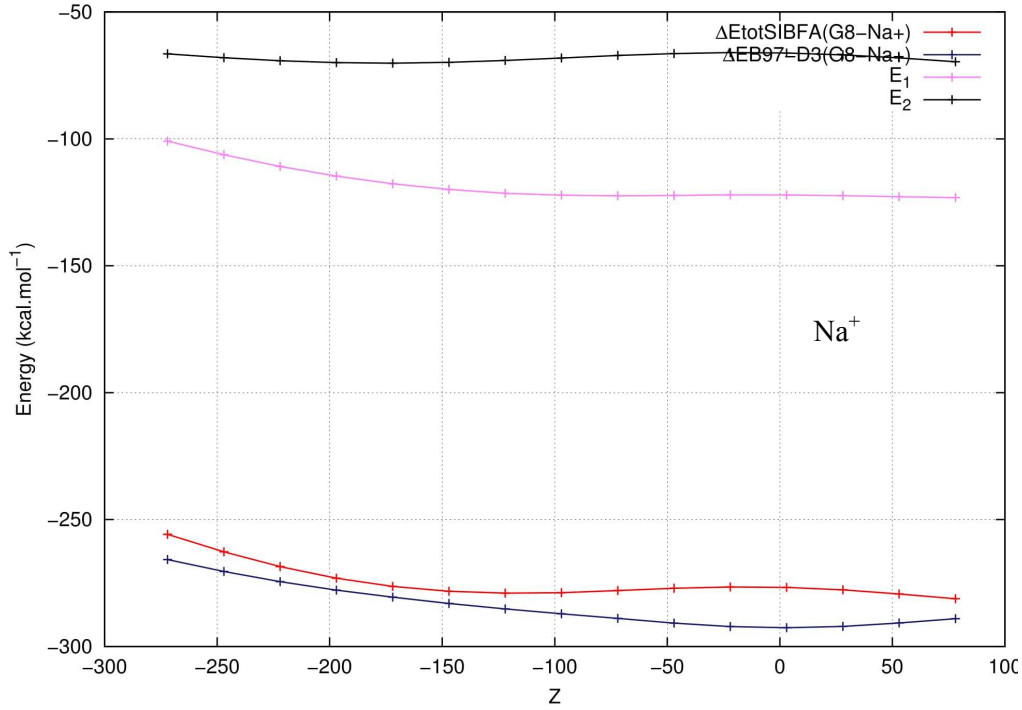
ΔEtotSIBFA(G8−Na+)
ΔEB97−D3(G8−Na+)
E1
E2
Na+
Energy (kcal.mol−1)
Z
−50
−100
−150
−200
−250
−300
−300
−250
−200
−150
−100
−50
0
50
100

(d)

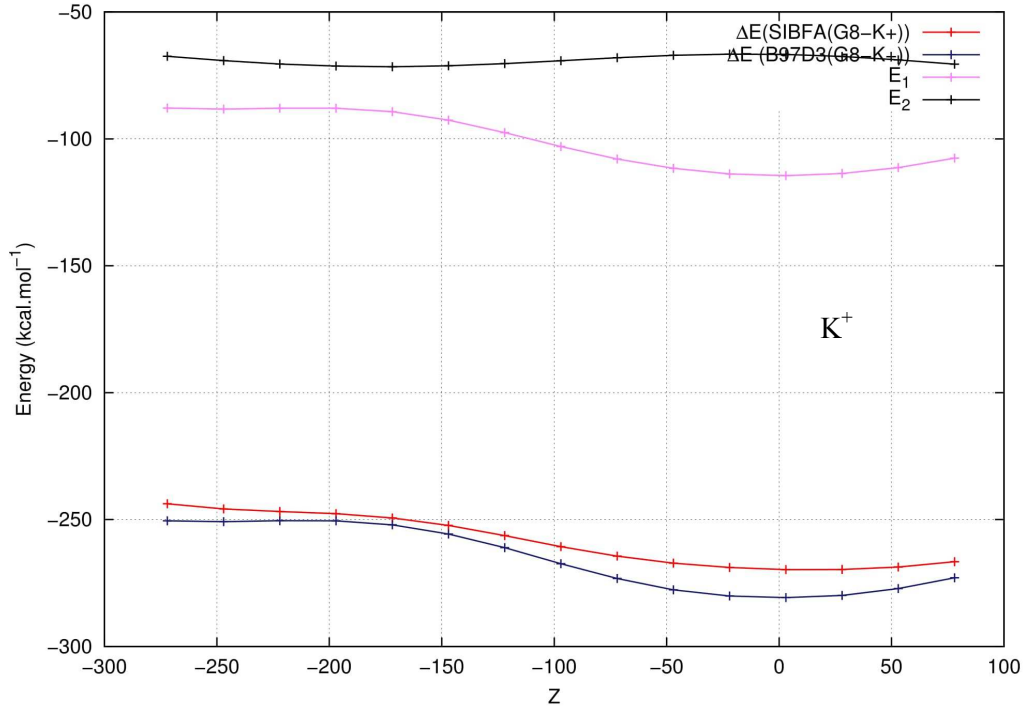
ΔE(SIBFA(G8−K+))
ΔE (B97D3(G8−K+))
E1
E2
K+
Energy (kcal.mol−1)
Z
−50
−100
−150
−200
−250
−300
−300
−250
−200
−150
−100
−50
0
50
100

(e)

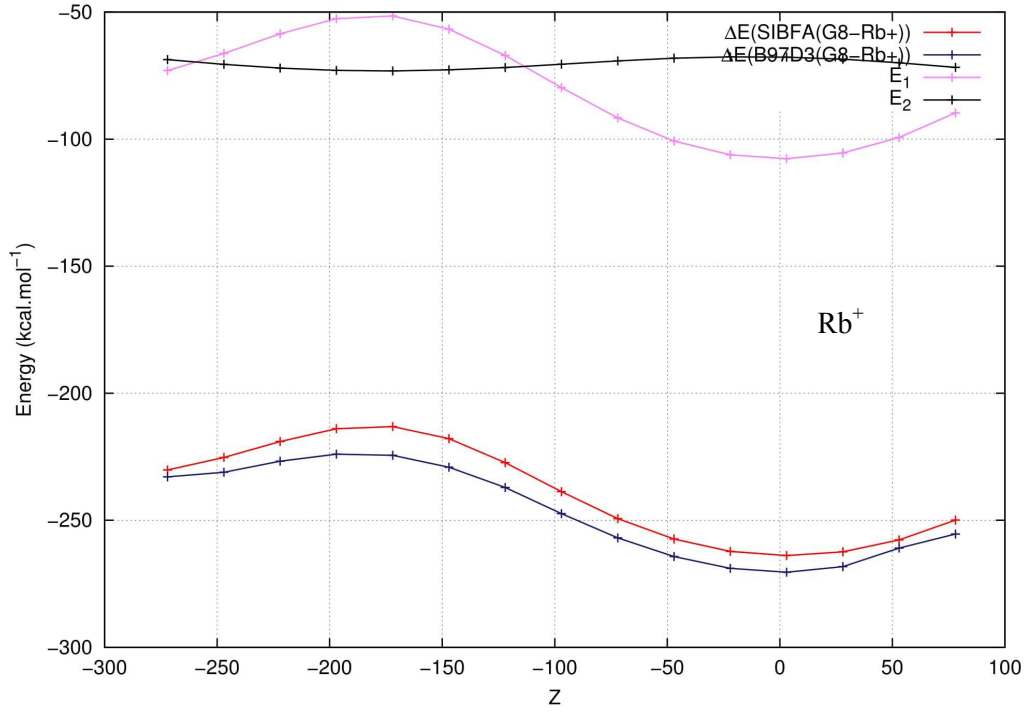

Figure 3. 3a: ΔE(B97-D3), ΔE(B3LYP-D3), ΔE_{tot}(SIBFA) and E_1/E_2(SIBFA) profiles for Li^+ channeling along the Z axis. 3b: ΔE(HF), ΔE(B3LYP) and ΔE(SIBFA) profiles for Li^+ channeling.
3c-3d: ΔE(B97-D3), ΔE(B3LYP-D3), ΔE_{tot}(SIBFA) and E_1/E_2(SIBFA) profiles for cation channeling along the Z axis. 3c: Na^+; 3d : K^+ ; 3e: Rb^+.
For clarity, the Z values along the abscissa (Å) were multiplied by a factor 100

(a)

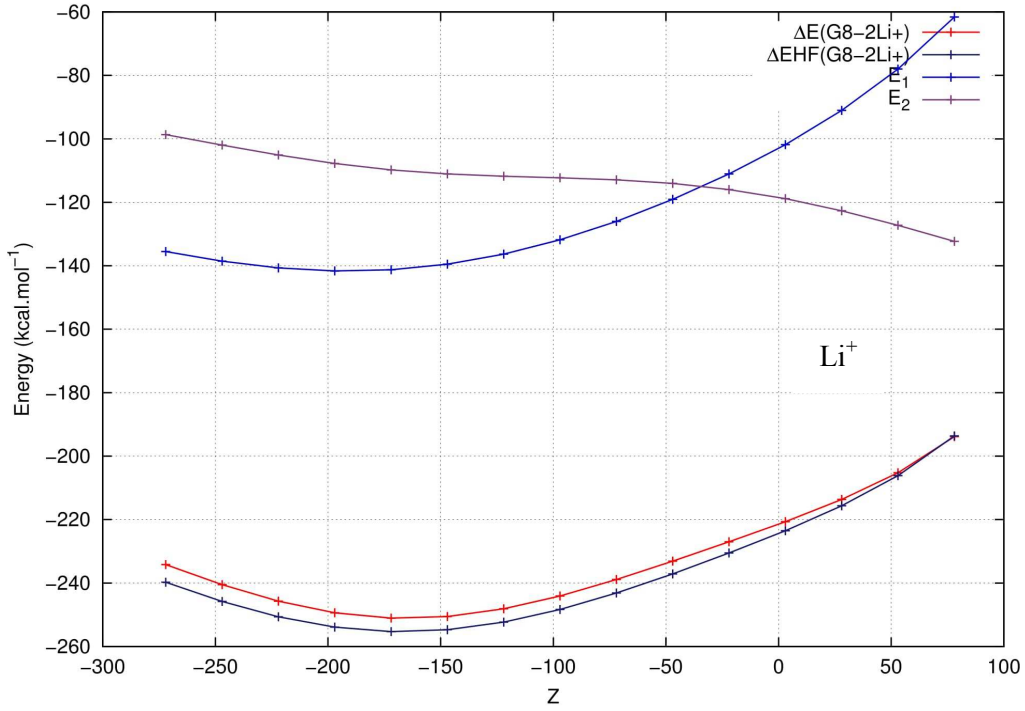
ΔE(G8–2Li+)
ΔEHF(G8–2Li+)
E1
E2
Li+
Energy (kcal.mol−1)
Z
−60
−80
−100
−120
−140
−160
−180
−200
−220
−240
−260
−300
−250
−200
−150
−100
−50
0
50
100

(b)

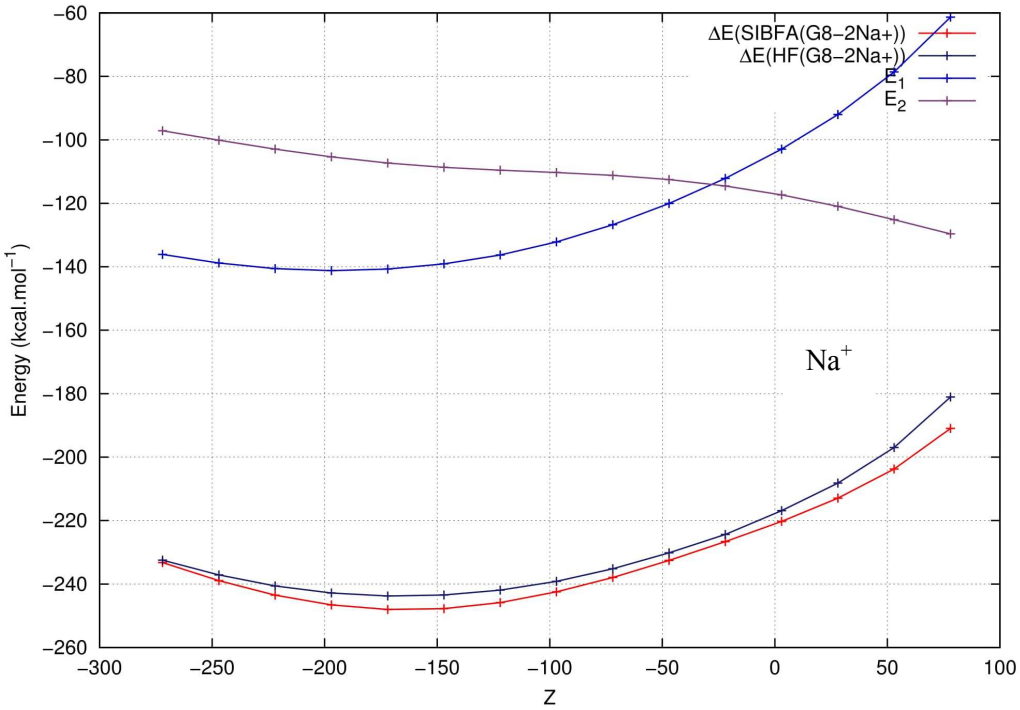
ΔE(SIBFA(G8–2Na+))
ΔE(HF(G8–2Na+))
E1
E2
Na+
Energy (kcal.mol−1)
Z
−60
−80
−100
−120
−140
−160
−180
−200
−220
−240
−260
−300
−250
−200
−150
−100
−50
0
50
100

(c)

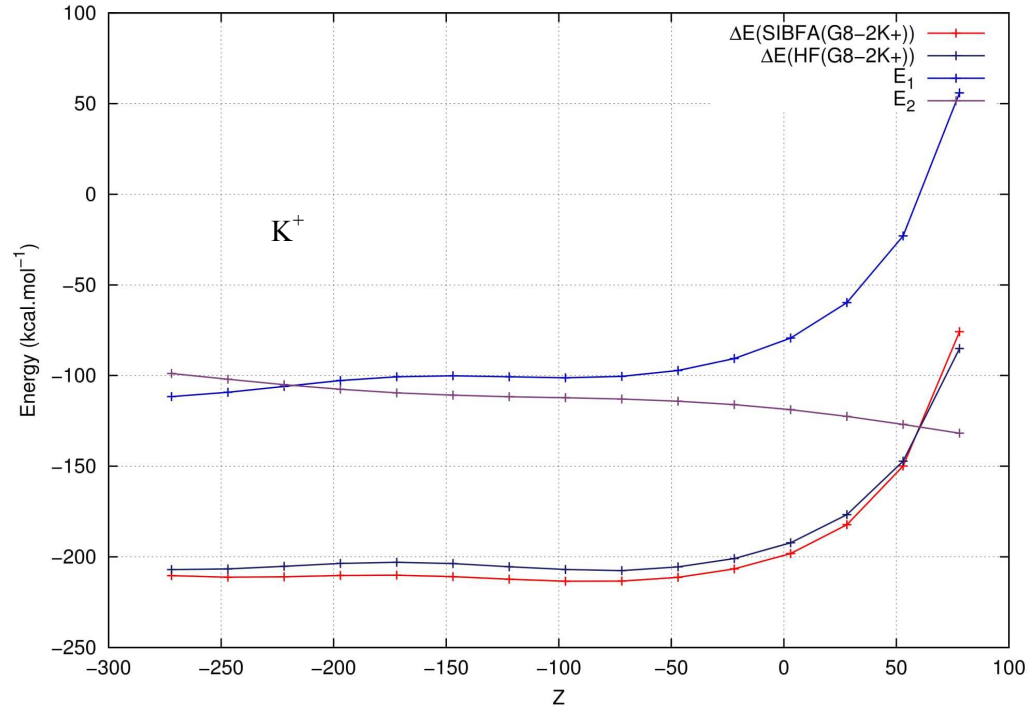

(d)

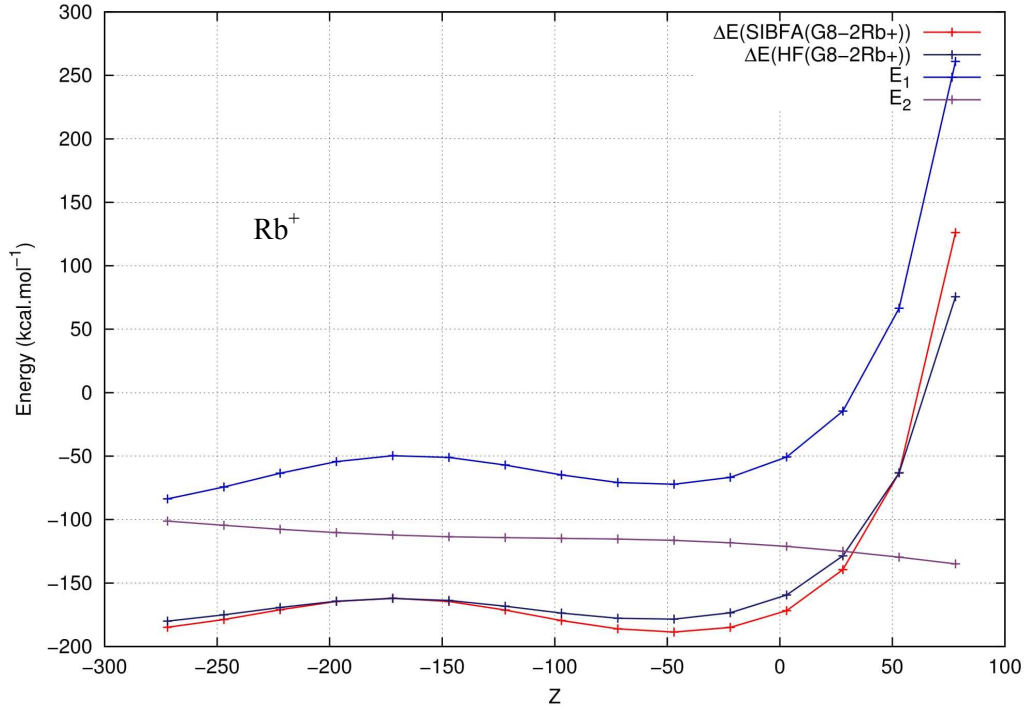

Figure 4. Complex of two stacked G quartets with two monovalent cations with one moving cation. ΔE(HF), ΔE(SIBFA), and E_1/E_2(SIBFA) profiles for cation channeling along the Z axis. 4a: Li^+; 4b: Na^+; 4c: K^+; 4d: Rb^+. For clarity, the Z values along the abscissa (Å) were multiplied by a factor 100.

(a)

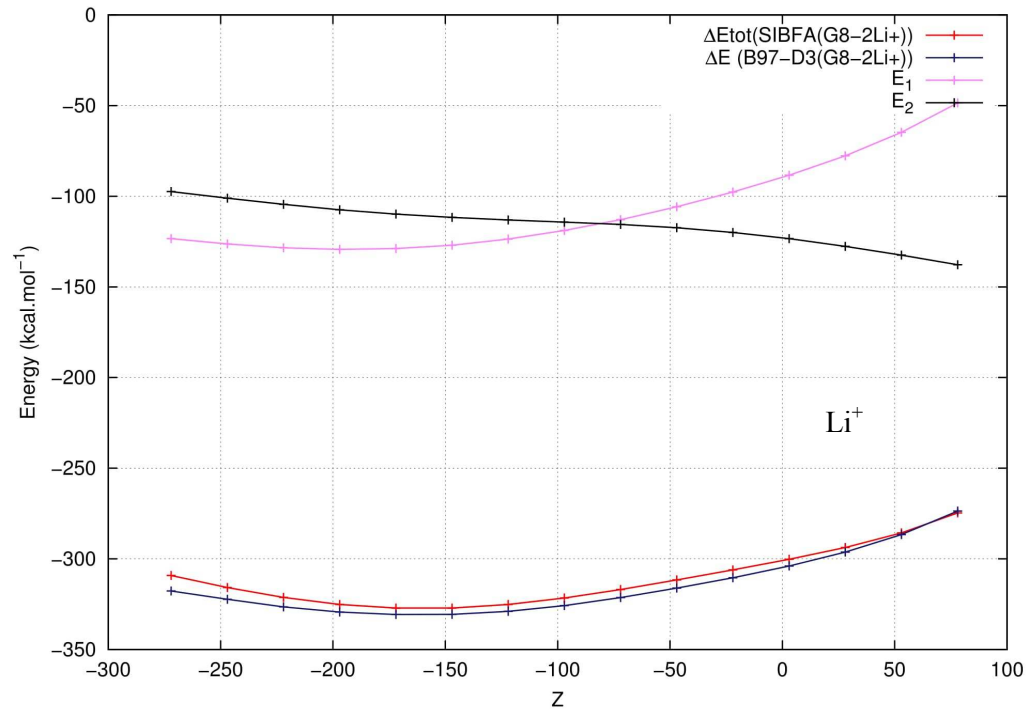
ΔEtot(SIBFA(G8−2Li+))
ΔE (B97−D3(G8−2Li+))
E1
E2
Li+
Energy (kcal.mol−1)
Z
0
−50
−100
−150
−200
−250
−300
−350
−300
−250
−200
−150
−100
−50
0
50
100

(b)

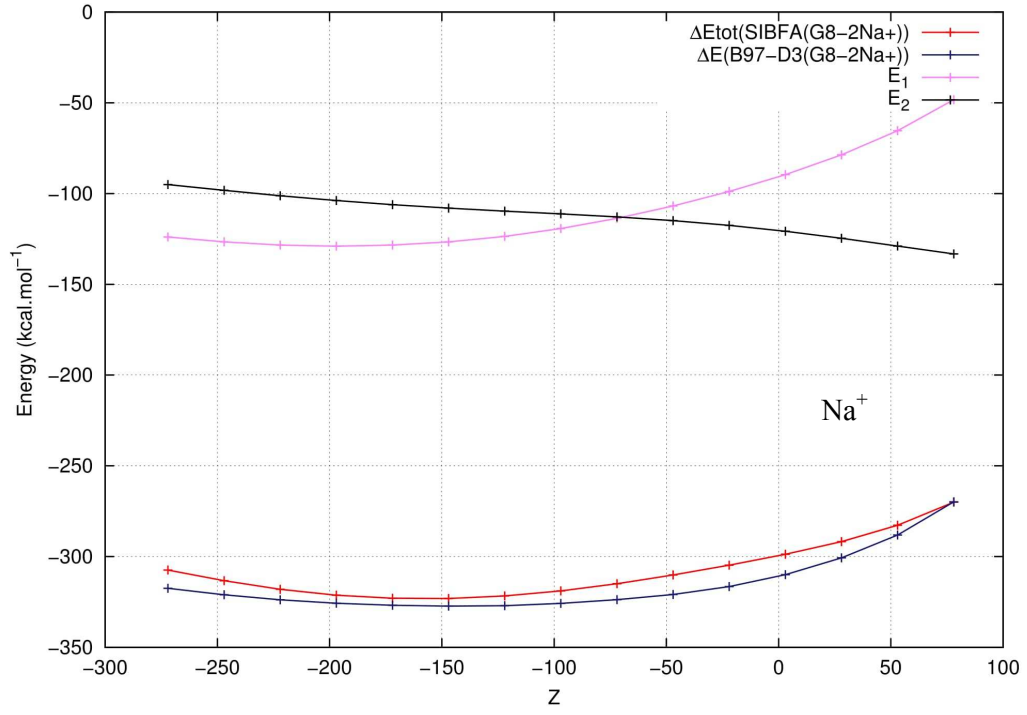
ΔEtot(SIBFA(G8−2Na+))
ΔE(B97−D3(G8−2Na+))
E1
E2
Na+
Energy (kcal.mol−1)
Z
0
−50
−100
−150
−200
−250
−300
−350
−300
−250
−200
−150
−100
−50
0
50
100

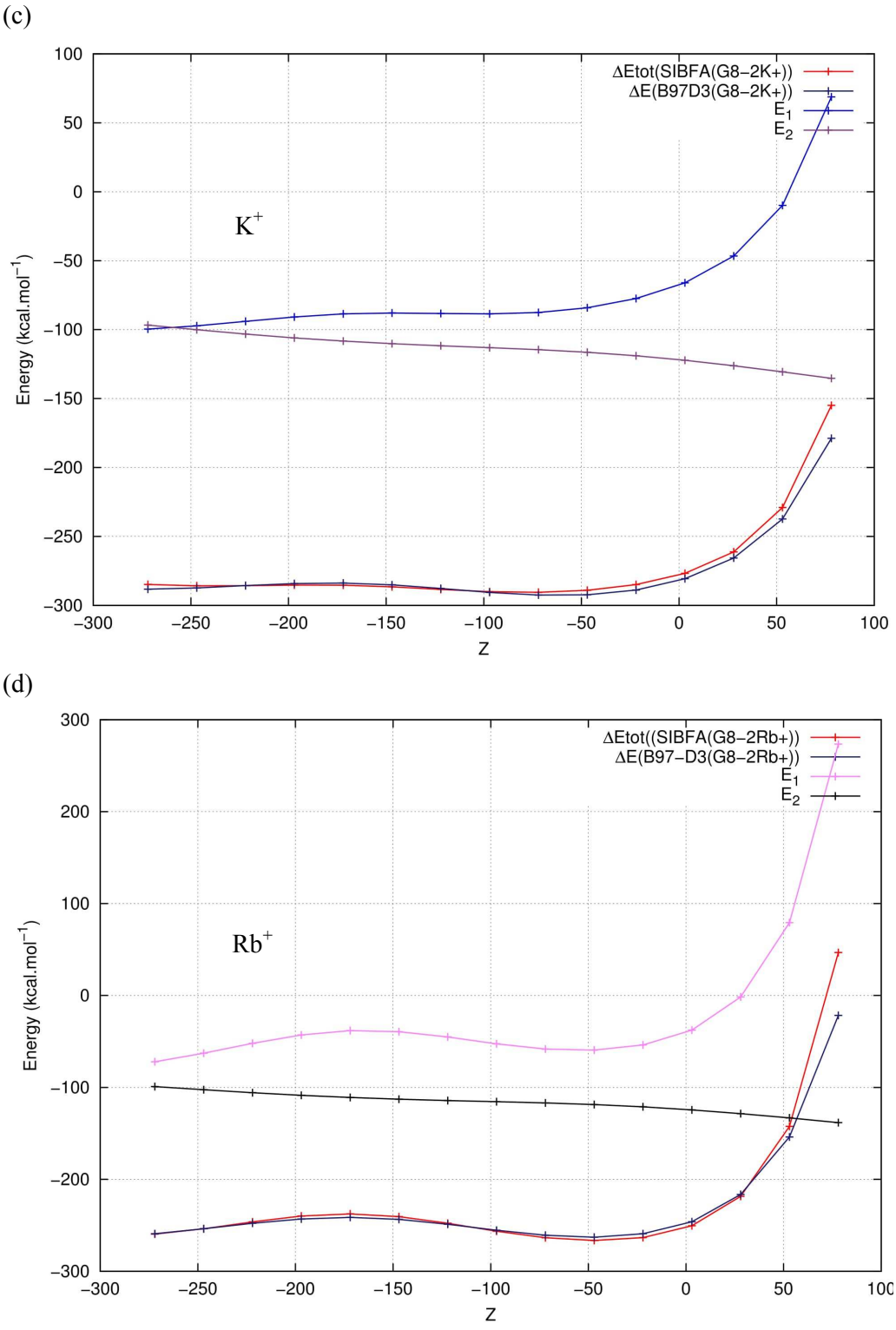

Figure 5. Complex of two stacked G quartets with two monovalent cations with one moving cation. ΔE(B97-D3), ΔE_{tot}(SIBFA), and E_1/E_2(SIBFA) profiles for cation channeling along

the Z axis.. 5a: Li^+; 5b: Na^+; 5c: K^+; 5d: Rb^+. For clarity, the Z values along the abscissa (Å) were multiplied by a factor 100.

(a)

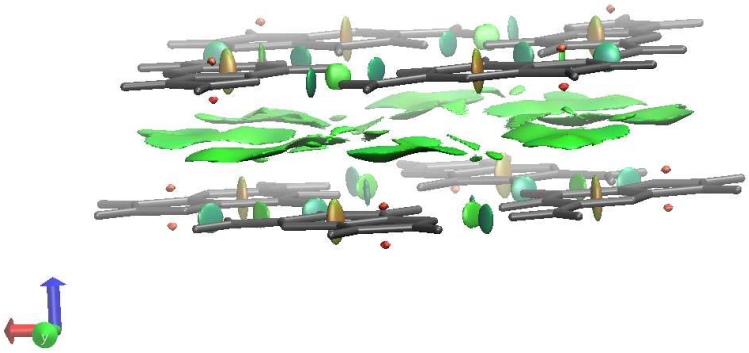

(b)

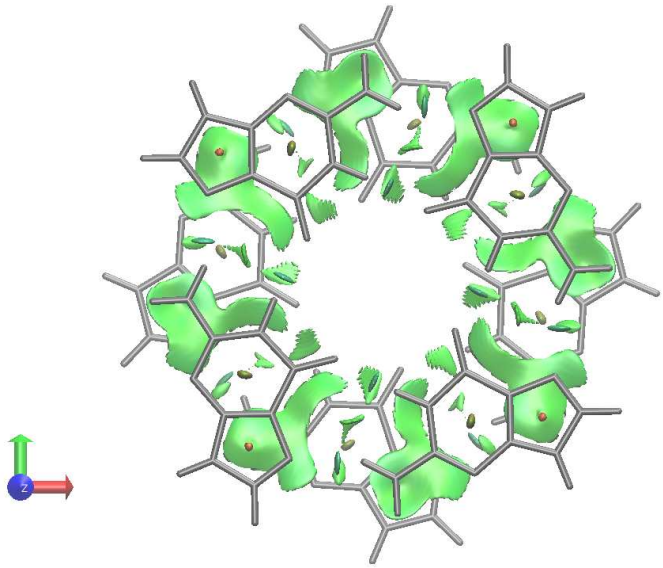

(c)

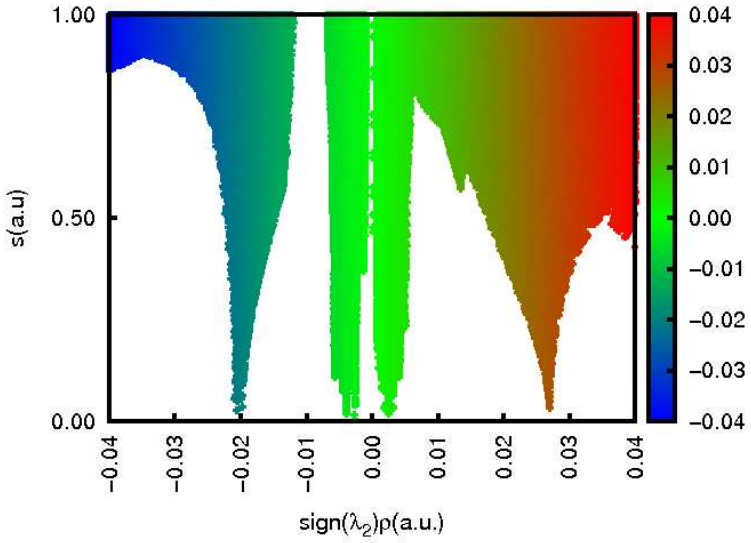

Figure 6. 3D plot NCI analysis of the two guanine quartets without cation: (a) in the XZ plane; (b) in the XY plane; and (c) corresponding 2D plot. In the 3D plots, the NCI surfaces correspond to s = 0.50 isosurfaces.

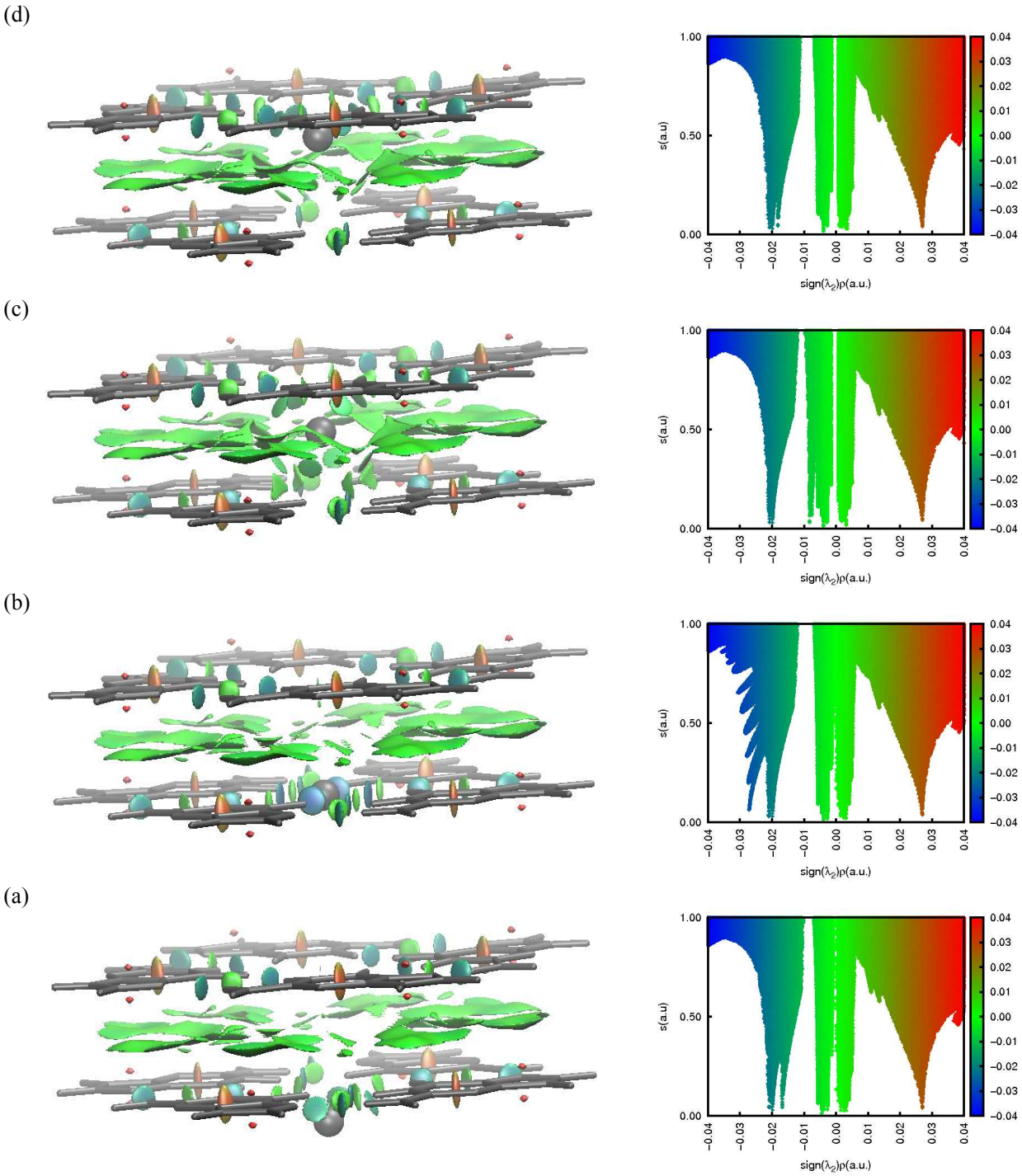

Figures 7a-d. 2D and 3D plot NCI analyses of the two guanine quartets with K^+ along the Z axis: (a): Z = -2.7 Å, (b): Z = -1.7 Å, (c): Z = 0.0 Å, (d): Z = 0.8 Å. In the 3D plots, the NCI surfaces correspond to s = 0.50 isosurfaces.

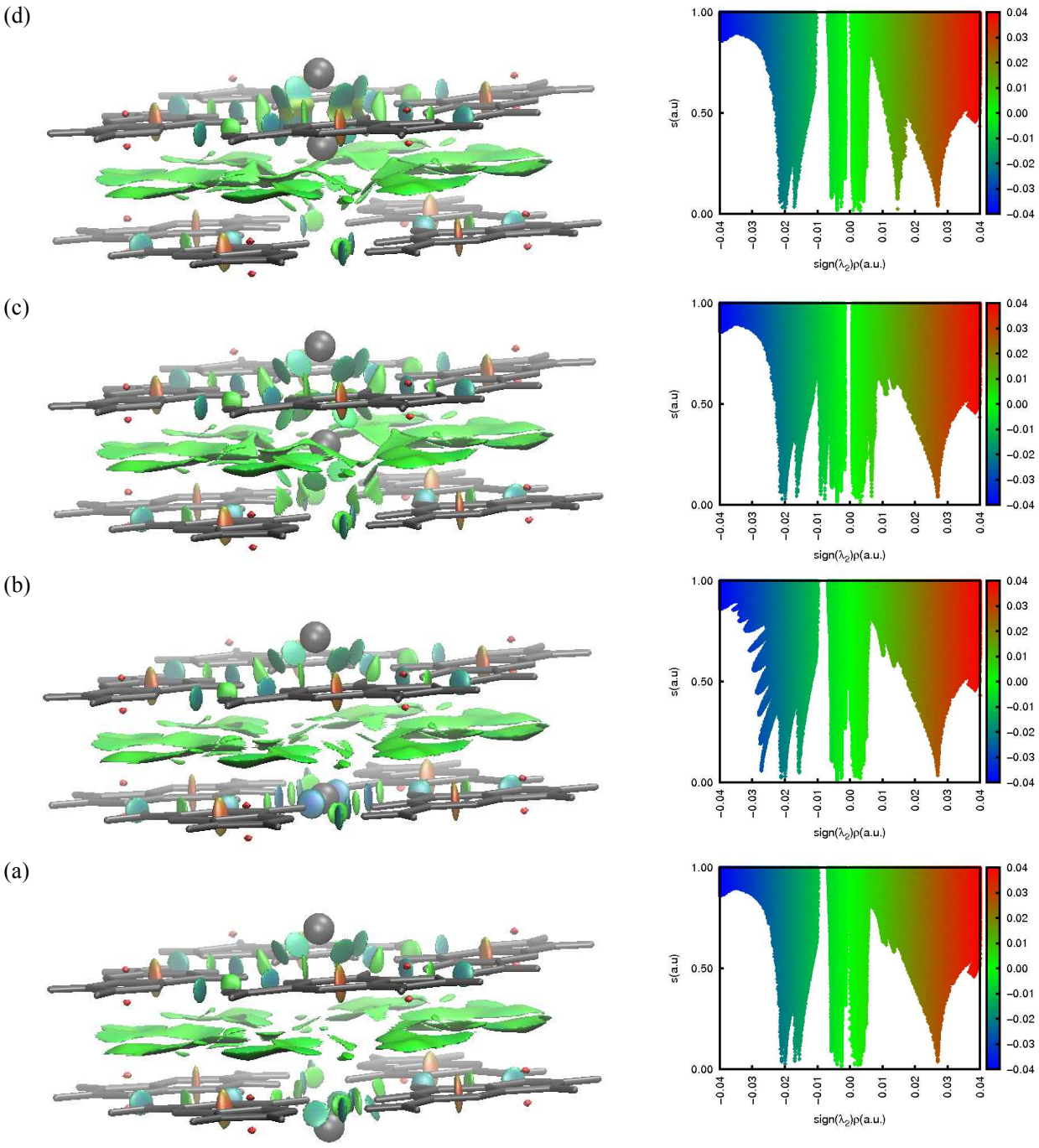

Figures 8a-d. 2D and 3D plot NCI analyses of the two guanine quartets with a fixed K^+ cation at Z = 2.8 Å and a mobile K^+ cation along the Z axis : (a): Z = -2.7 Å, (b): Z = -1.7 Å, (c): Z= 0.0 Å, (d): Z= 0.8 Å. In the 3D plots, the NCI surfaces correspond to s = 0.50 isosurfaces.